Christoph Edelsbrunner, BSc

Multi-scale biomechanical investigation of human aortas by means of multi-photon microscope imaging with simultaneous biaxial extension test

MASTER'S THESIS

to achieve the university degree of

Master of Science

Master's degree programme: Biomedical Engineering

submitted to

Graz University of Technology

Supervisor

inz. mgr inz. Anna Pukaluk
Ass.Prof. Dipl.-Ing. Dr.techn. Gerhard Sommer

Institute of Biomechanics
8010 Graz, Stremayrgasse 16/II

Head
Univ.-Prof. Dipl.-Ing. Dr.techn. Gerhard Holzapfel

Graz, October 2019

Affidavit

I declare that I have authored this thesis independently, that I have not used other than the declared sources/resources, and that I have explicitly indicated all material which has been quoted either literally or by content from the sources used. The text document uploaded to TUGRAZonline is identical to the present masters thesis dissertation.

—————————————————
date

—————————————————
signature

Contents

Abstract

In biomechanics, the biaxial extension test is one of the most frequently used tests to provide information about physiological and pathological behavior in human arteries. If such a test is performed under a multi-photon microscope, one does not only receive feedback about the mechanics of the artery but also makes it possible to observe the changes in the microstructures within an artery. The main focus of this master thesis is on two structure proteins: collagen and elastin. Only atherosclerotic and aneurysmatic human specimens are used. For the analysis, each time the stretch level is increased by the biaxial extension machine, two images with different emission wavelengths are taken, each representing one of the structural proteins. To achieve the best possible evaluation with this specific setup, the appropriate autofluorescence excitation and emission wavelength is first sought in human and porcine tissues by the means of confocal microscopy. The tissue is also stained with fluorescent microspheres to observe the stretch conditions within the tissue and during the experiment. To further improve the results, confocal reflection microscopy was tested in addition to collagen analysis. Finally, a qualitative analysis of the diameter, orientation and tortuosity of collagen and elastin fibers is performed with all the collected data from multiphoton microscopy. All these data are also evaluated statistically for the reason to be aware of any similarities or differences.

Experimental data show a collagen emission wavelength of 460 nm for the multiphoton laser excitation and 567 nm for Ar-laser excitation. Contrary, the emission wavelength for elastin is higher for both excitation methods. The emission wavelength for excitation with the multiphoton laser is 525 nm and for the Ar-laser this is 590 nm. It is also shown that elastin has a higher intensity of autofluorescence and confocal reflection microscopy can only be used for investigating collagen. Cauchy stress-stretch diagrams of the different samples prove that aneurysmatic tissue is stiffer than atherosclerotic tissue. As far as the dispersion of the fiber angle is concerned, it can be said that the fibers initially are widely dispersed in a certain direction, but with increasing stretch level, they tend to a more anisotropic behavior into that direction. The statistical evaluation shows a remarkably high monotonic relationship between the three parameters diameter, amplitude and tortuosity.

Zusammenfassung

In der Biomechanik wird ein biaxialer Zugversuch eingesetzt um Information über das physiologische und pathologisches Verhalten der Arterie zu erlangen. Führt man diesen Zugversuch zusätzlich unter einem Multiphotonen-Mikroskop durch, erhält man zum einem Rückschlüsse über das mechanische Verhalten der Arterie und zum anderen sind Veränderungen der Struktur des Gewebes im mikroskopischen Bereich zu beobachten. Das Hauptaugenmerk dieser Arbeit liegt dabei auf der Veränderung der beiden Strukturproteine Elastin und Kollagen. Dazu wird atherosklerotisches und aneurysmatisches menschliches Gewebe untersucht. Zur Analyse werden während des biaxialen Zugversuchs mikroskopische Bilder mit zwei verschiedenen Emissions-Wellenlängen aufgenommen. Jeweils eine der beiden emittierten Wellenlängen repräsentiert ein Strukturprotein. Um den Emmissions-Wellenlängenbereich für den bestehenden Versuchsaufbaus zu finden, wird anfangs das Autofluoreszenz-Spektrum von tierischem und menschlichem Gewebe mit der Konfokal-Mikroskopie gesucht. Zusätzlich wird der Einsatz der Möglichkeit der konfokalen Reflexionsmikroskopie getestet. Mit einer Gewebefärbung werden fluoreszierende Referenzpunkte im Gewebe erzeugt um die lokalen und globalen Spannungsverhältnisse zu erkunden. Um Ähnlichkeiten bzw. Unterschiede zwischen Durchmesser, Orientierung und Welligkeit im Gewebe zu erkennen, werden die verschiedenen Parameter zunächst berechnet und anschließend statistisch bewertet.

Die ermittelten Daten zeigen eine Emissions-Wellenlänge für Kollagen von 460 nm bei Anregung mit dem Multiphotonen-Laser und 567 nm bei Anregung mit dem Ar-Laser. Die Emissionswellenlänge für Elastin liegt bei beiden Anregungsmethoden höher mit 525 nm bzw. 590 nm. Zusätzlich wird bewiesen, dass Elastin eine stärkere Intensität der Autofluoreszenz aufweist und mit der konfokalen Reflexionsmikroskopie nur Kollagen nachgewiesen werden kann. Das Spannungs-Dehnungs-Diagramm zeigt dass sich aneurysmatische Arterien steifer verhalten als atherosklerotische. Die Verteilung der Ausrichtung der einzelnen Kollagen- und Elastin-Fasern im Gewebe ist zu Beginn stärker in eine bestimmte Richtung gestreut. Die Fasern neigen dazu, sich mit zunehmender Dehnung anisotrop in diese Richtung zu orientieren. Die statistische Auswertung weist auf eine hohe monotone Korrelation zwischen den Parametern Faser-Durchmesser, Welligkeit und Welligkeits-Amplitude hin.

Acknowledgment

First of all, I want to thank my supervisors Anna Pukaluk and Gerhard Sommer for their expertise, guidance, and truly friendly support throughout the process of writing the thesis. Your way of teaching me things made it a lot easier for me to finish it. Additionally, I offer my sincerest gratitude and thanks to Prof. Holzapfel as the head of the Institute of Biomechanics for the opportunity to work in this interesting field and finish my study at the Technical University of Graz.

Very special thanks go out to my parents, Gerlinde and Andreas. Whenever I needed help to maintain the motivation for my study, you two were here for cheering me up. You always gave me enough strength to care about my degree and pushed me to finish it.

Last but most definitely not least I want to thank my brother Lukas, whenever it was time to take me to other thoughts outside of the study, you were the right person for it.

1. Introduction

In this chapter the motivation for the master thesis is shown. This should provide a better insight and explain the benefits of this study. Human arteries consist of three different layers, which are mainly made out of the structure-proteins elastin and collagen. In addition to these two proteins, other components like endothelial cells can be found in the tunica intima, smooth muscle cells in the tunica media or proteoglycans in every layer. The interaction of all these different components is essential to understand the mechanical response of the tissue. It is important to recognize each of these structures separately through different imaging processes in loaded and unloaded conditions. Different characteristics of the proteins are investigated and statistically analysed. This work shows the close interaction between biology and engineering.

1.1. Motivation

Knowledge of biomechanical properties of the arterial wall is important for several reasons. It offers insight into developments of diseases (Holzapfel et al., 2004) or is needed to design parameters for artificial tissue (Knoener et al., 2006). With a biaxial extension test the physical load conditions of an artery can be imitated very well. Normally, Cauchy stress-stretch curves of the different layers of the artery were obtained in physiological or pathological conditions shown by Lima et al. (2015) and Holzapfel et al. (2004). However, the stress-stretch curves gave feedback of the mechanical properties of the whole sample, consisting of structure proteins like collagen and elastin or smooth muscle cells.

It is not only the response of the entire tissue that is interesting, but also how the individual structural proteins behave in it. So the idea came up to combine a biaxial extension test with a simultaneous investigation by means of a multiphoton microscope imaging technique. Therefore, a biaxial extension test machine was designed to fit onto the multiphoton microscope. This machine was already built by the *Institute of Biomechanics*. This experimental set-up made it possible to observe the changes in the structural parameters separately, with particular attention to the two proteins collagen and elastin. This has the advantage that the changes in structure of the aorta can be observed from the initial unloaded stage up to an increased stretch level.

1.2. Goal of this thesis

The goal of this thesis was to detect the changes in different parameters of collagen and elastin fibers during a biaxial extension test to understand the mechanical response of the entire tissue. In order to be able to accurately detect various parameters of those proteins, the autofluorescence of collagen and elastin were examined with confocal microscopy more closely at the beginning. It was about finding the right excitation and emission wavelength that were best suited for this experimental setup. This was initially tested with porcine aorta and then with human aorta. During this experiment, information on the intensity of autofluorescence of the two proteins was also obtained. The possibility of confocal reflection microscopy was also investigated. With this method it was possible to detect collagen without autofluorescence to distinguish between elastin and collagen tissue. Fluorescent microspheres were used to stain the tissue. This was needed to determine data which allows to make statements of the stretch ratios within the sample.
Finally multiphoton microscopy images of pathological human samples were acquired. Once the collected data have been recorded, they should be analysed. For this purpose Cauchy stress-stretch diagrams were created, the change of diameter, waviness and amplitude were evaluated. In addition, the change of the angle of fiber direction of collagen and elastin were described. Finally, all these data were statically assessed to discover similarities or differences.

This work takes place in the framework of the *Multiscale Biomechanical Investigation of Human Aortas* by the *Institute of Biomechanics* at the *Grat University of Technology*.

2. Materials and Methods

In this chapter the methods of working, the instruments, the materials and tissues are introduced. The main focus is on the use of the microscope and its three operation methods: confocal microscopy, confocal reflection microscopy, and multiphoton microscopy. The usage of the main testing device, the biaxial tensile testing machine, is also explained. In the further process the methods are explained with which the structural parameters like fiber diameter were computed. Lastly, the statistical methods used are clarified.

2.1. Layer separation, preparation and mechanical testing

All elastic human arteries have basically the same wall structure if their lumen exceeds a certain diameter. The artery can be divided into three sections: tunicia intima, tunica media and tunica adventitia. The intima is the innermost layer, whereas the adventitia is arranged on the outside of the artery. Every single layer of an artery offers different mechanical properties (Holzapfel et al., 2004).

The arteries were supplied by the *Institute of Pathology* from *Medical University of Graz* as a whole piece with a length up to 10 cm and were snap frozen. To separate the layers, the samples are thawed at $4°$ C on the previous day. The layer separation is executed with the help of a scalpel, a pair of tweezers and a pair of scissors. At the beginning the scissors are inserted into the opening of the artery and the vessel wall is severed on one side. The initial tube shape of the artery now exists as a plane. Figure 2.1 depicts this state for the three human samples which were investigated.

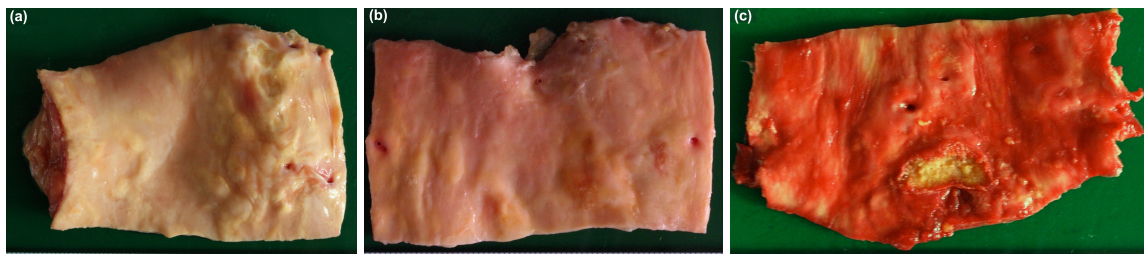

Figure 2.1   The pictures show the cut abdominal aortas with the initmal side up. **(a)** shows the atherosclerotic aorta from Person #3, Sample 1, **(b)** depicts Person #3, Sample 2, and **(c)** pictures the aneurysmatic aorta from Person #2.

After removing loose connective and lipid tissue on the in- and outside of the opened artery, the sample has to be brought to the correct size in the next step. The biaxial tension machine is designed for a $20\,mm \times 20\,mm$ sample. Therefore, the tissue is put into a punch press which cuts the tissue down to the mentioned size. Right after the layers can be separated. The tissue is fixed in the machine by 20 hooks. Five hooks on every side of the tissue. The correct place for positioning the hooks is transferred to the tissue using a template and a surgical marker. Finally, the five hooks were pierced through the marked positions with a suture thread attached to them. The suture thread allows the fixation in the biaxial tension machine.

Additionally porcine samples were used. The porcine arteries were bought at a local slaughterhouse. The wall structure can be described with a two-layer model. So there are only the intima-media layer and the adventitia layer as stated by Wang et al. (2004). If tests were done with a porcine sample, the procedure was very similar as mentioned for human tissue. The only difference was that during the layer separation, the endothelial tissue was removed. This was necessary in order to create a surface for the staining which is similar to the surface of a human media. Table 2.1 lists all tested porcine and human samples. The table provides information on which donor the sample came from and which technique was used to obtain the microscopic images. Table 2.2 provides further biological and pathological information on human samples. Five human media samples were prepared from three different donors. Two different parts of the abdominal aorta from *Person #1* were treated with elastase and collagenase, respectively. Also two different samples were taken from the abdominal aorta of *Person #3*. The numbering from Table 2.2 is also used in the further course to identify the related tables, diagrams and images.

Table 2.1   Tested samples and corresponding image acquisition technique.

Confocal microscopy	Confocal Reflection microscopy	Multiphoton microscopy
1 porcine intima-media	1 porcine intima-media	3 human media
1 porcine intima-media stained with TetraSpeck	1 porcine adventitia	
1 human media treated with collagenase	1 human media treated with elastase	
1 human media treated with elastase	1 human media treated with collagenase	

The mechanical tests were performed with the computer-controlled biaxial tensile testing machine. The biaxial tensile machine was designed and manufactured by the *Institute*

Table 2.2   Biological and pathological information about the donors.

Person	Age	Aorta section	Sex	Level of atherosclerosis	Aneurysmatic
#1	53	abdominal	male	medium	no
#2	81	abdominal	male	high	yes
#3	80	abdominal	male	high	no

of Biomechanics at the *Graz Technical University*. A photograph of the machine with attached sample can be seen in Figure 2.2. In this picture, the testing device was already placed on the microscope. The movements are controlled by four high precision linear
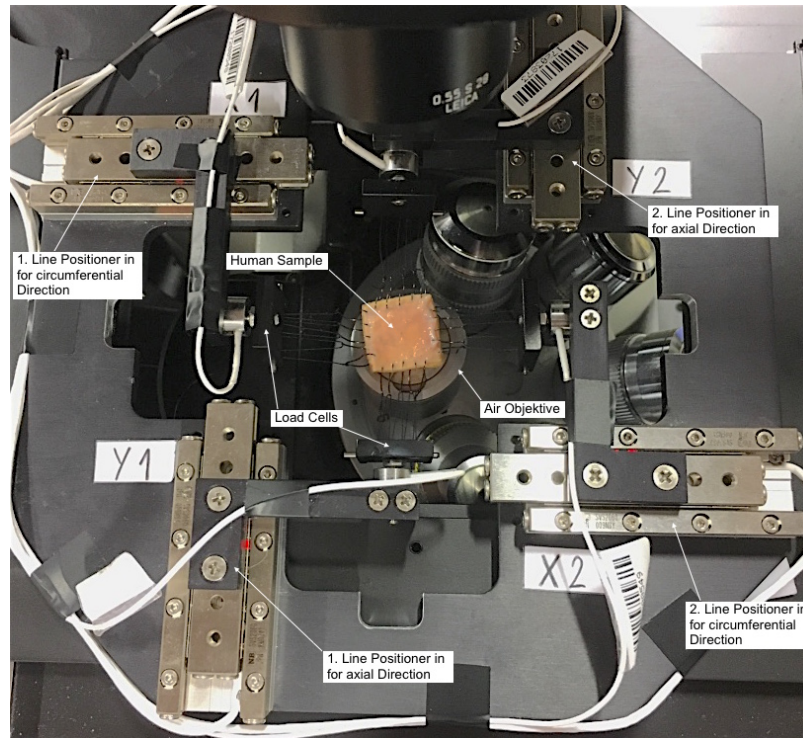

Figure 2.2   Picture of biaxial tensile machine with attached sample before testing with multiphoton microscope

positioners *SLC-2460* (SmarAct GmbH, Geramy). The advantage of this linear positioner is the resolution of less than 1 nm. The load cells *KM10z - 25N* (ME-Meßsysteme GmbH, Germany) can be loaded with maximal 25 N. With a GUI from the program *LabView* (National Instuments, USA) the stretch can be controlled which is applied on the sample. The sample is mounted on metal pins on the load cell around which the suture thread is evenly wound. The load cells allow the read out of the force applied onto the tissue. With this data a Cauchy stress-stretch diagram can be computed (see subsection 3.3.1). Afterwards the biaxial testing machine with the sample is placed on the confocal microscope *TCS SP5* (Leica Microsystems GmbH, Germany). The *TCS SP5* is equipped with a multiphoton laser of the type titanium-sapphire laser. This microscope allows taking images with confocal microscopy, confocal reflection microscopy or multiphoton microscopy method.

Before every image acquisition preconditioning was performed. Preconditioning is necessary because the typical visco-elastic response of the arterial tissue is different during the first load cycles due to tissue softening (Holzapfel et al., 2001). To investigate the local stretch conditions, the selected sample was tested with fluorescent microspheres. In this

case, they were applied to the specimen immediately before preconditioning. *TetraSpeck Fluorescent Microsphere Standards* (Thermo Fisher Scientific, USA) were used. This stain contains four different fluorescent types. The excitation/emission peaks range from 365/430 nm to 660/680 nm (TertaSpeck User Manual , 2001).

2.2. Confocal microscopy

To detect the autofluorescence of elastin and collagen in porcine and human samples, the *TCS SP5* was run in confocal microscopy mode. Following excitation wavelengths from the argon-laser can be used: 458, 476, 488, 496, 514, 561, 594 and 633 nm with an maximal output power of 200 mW. To get starting points for the corresponding excitation and emission wavelengths for collagen and elastin a literature review was conducted to see what imaging-techniques allow a tissue analysis at VIS-light excitation. The results are listed in Table 2.3.

Table 2.3   Different settings from various authors according the excitation and emission wavelength of elastin and collagen autofluorescence

Paper	Fitzmaurice et al. (1989)	Richards-Kortum et al.(1996)	Deyl et al. (1980)	Gill et al. (2003)
Collagen				
Ex [nm]:	476	330 ; 450		365; 440
Em [nm]:	barrier filter at 515	390; 530		465; 520
Elastin				
Ex [nm]:	476	410 ; 450	340	
Em [nm]:	barrier filter at 530	500; 520	410	
Sample:	human	human	human	human
Paper	O'Connel et al. (2008)	Croce and Bottiroll (2014)	Stephen et al. (2013)	Zhao et al. (2017)
Collagen				
Ex [nm]:	514	330 - 340		488
Em [nm]:	500 - 530	400 - 410		548
Elastin				
Ex [nm]:	488	350 - 420	405	
Em [nm]:	420 - 510	400 - 410	500 - 550	
Sample:	rat	rat	human	human

For the measurement of the emission spectrum a Stoke's shift with a typical value between 20 and 100 nm was considered (Alfano and Yang, 2003). For the detection of the emission which was created by the argon-laser, a photomultiplier tube was used. The photomultiplier tube allows the wavelength spectrum to be measured to be changed very easily. If the microscope was run in *Photon-count* mode, the hybrid detector was used. The hybrid detector is the combination of a photomultiplier and a microelectronical photo diode. This modus can exactly tell how many photons are collected in the spot of one pixel. The brighter one pixel appears in the image, the higher is the amount of collected photons at this place (Leica Hybrid detection for Confocal Imaging, 2011).

2.2.1. Autofluorescence of porcine sample

As one can see from Table 2.3 there are different possibilities to adjust the excitation and emission wavelength to detect collagen or elastin according to different authors. In the beginning, the proposed adjustments were still adhered to, but it soon became apparent that this was not the right approach. For this reason, a test with all possible wavelengths was performed on a porcine artery to determine the appropriate settings for this microscope. The excitation was performed with all possible wavelengths and combinations of different wavelengths. The results can be observed in subsection 3.1.1.

2.2.2. Autofluorescence of human sample

The porcine sample was replaced by two human media samples which were treated with elastase and collagenase, respectively. Elastase treated samples have only collagen structures in it after the treatment. The opposite applies to collagenase treated samples. This treatment made it possible to clearly distinguish between collagen- and elastin-emission. The excitation wavelengths got varied for both samples and the resulting autofluorescence images got compared. With the knowledge of the suitable excitation wavelength, a subsequent lambda-scan was performed with the *Leica SP5* for the two proteins. A lambda-scan is advantageous for the detection of autofluorescence if the emission spectrum is unknown. A lambda scan allows you to scan a fluorescent sample over a desired emission wavelength range. Additionally it is helpful for the detection of the emission maximum. The spectrum investigated was between 525 nm and 700 nm for the autofluorescence of collagen with a step size of 8.33 nm. Since the excitation wavelength for elastin was set higher the starting wavelength of the spectrum was increased to 575 nm, which resulted in a step size of 5 nm. The autofluorescence microscopy pictures as well as the plots of the lambda-scans are depicted in subsection 3.1.2.

2.2.3. Intensity of elastin and collagen autofluorescence

This test with samples which are elastase- or collagenase-treated concerns the intensity of autofluorescence. Brightman et al. and Fitzmaurice et al. claim that there is a up to 25% higher autofluorescence intensity at elastin-only tissue compared to collagen-only tissue (Fitzmaurice et al., 1989; Richards-Kortum and Sevick-Muraca, 1996). To verify these statements the Leica SP5 was used in the *Photon-Count* modus.
To get discrete values and be able to compare the autofluorescence-intensity of collagen and elastin, the background corrected total fluorescence was calculated. In this process, the intensity of the autofluorescence of collagen or elastin was calculated at different areas of the sample. The background fluorescence was subtracted from the values in order not to falsify the result. Therefore the Analyze-Menu in *ImageJ* (National Institutes of Health, USA) was used to read out three parameters. These parameters were the selected *Area*, the *Mean Gray Value (MGV)* and the *Integrated Density (IntDen)*. The recorded images have a size of 16 bits, which results in 2^{16} different gray values. A Gray Value of 0 indicates

black, where as a Gray Value of 65535 would in this case be the maximum amount of light which can be recorded. It is represented in the images as white. The *Mean Gray Value* is the sum of the gray values of all the pixels in the selection, divided by the number of pixels from the selected *Area*. This value represents the optical density. There is no specific unit for it, it just indicates the quantity of brightness. The *Integrated Density(IntDen)* is just the product of the selected area *Area* and the *Mean Gray Value*. To calculate the *Background Corrected Total Fluorescence (BCTF)* one gets

$$BCTF = IntDen - (Area \cdot MGV) \tag{2.1}$$

which was shown by A. Burges et al. (2014).

To verify this results the height of mean emission of photons per pixel were additionally calculated in *Matlab* (TheMathworks Inc., USA). Therefore the pictures were loaded into the program to get the corresponding matrix. This matrix represents every pixel of the picture. Each element of the matrix describes the amount of photons at a certain pixel. To compare the intensity of collagen and elastin, all pixels which did not count a photon got deleted. Only pixels with at least one photon in it, contribute to the result. This enables the average height of photon emission to be examined and not just their total sum to be compared. The results got compared in Figure 3.7.

2.2.4. Analysis of local and global stretch

This part of this thesis includes the testing of porcine samples which were stained with fluorescence microspheres. The microspheres are needed to get reference points for the calculation of local stretch. Microspheres attach to the tissue and change their position due to the global stretch applied by the biaxial testing machine on the outside of the sample. So it is possible to calculate the local stretch in the middle of the tissue in contrast to the global stretch at the outside. In order to calculate the local stress, the exact position of two points of the microspheres were determined. For the calculation, the center of the sphere was determined and Pixel values were used for the calculation. Then the described path of the points in x- and y-direction was considered, which changed with every increase of global stress. In Figure 2.3(a) one can see that the horizontal and vertical distance between microsphere B_1 and B_2 are named x_0 and y_0, respectively. This is the distance in horizontal and vertical direction between the two microspheres in an unloaded situation. In Figure 2.3(b) a situation with a *global stretch* value of 2% is illustrated. Due to the stretching of the tissue the distances x_0 and y_0 get extend by Δx_0 and Δy_0.

To calculate the change of strain in percentage values, the new longer distance $(x_0 + \Delta x_0)$ must be divided by the initial distance (x_0). This lead to Equation 2.2 which defines the value of the stretch. The equation is the same for both x- and y-direction.
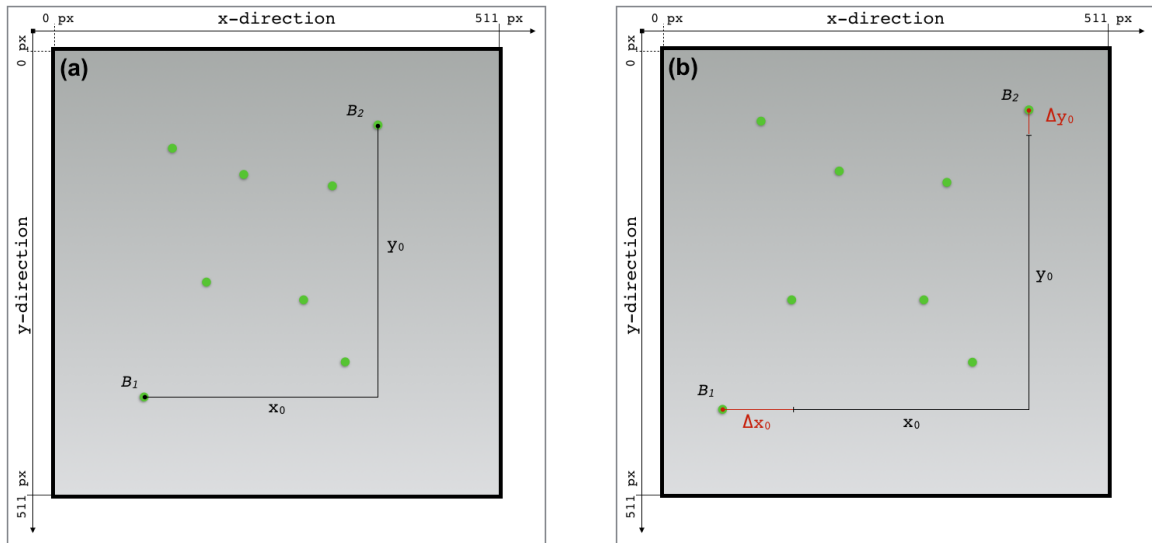
$$\lambda = \frac{x_0 + \Delta x_0}{x_0} \tag{2.2}$$

Figure 2.3 **(a)** Initial distances between two reference points *B1* and *B2* compared to **(b)** the distances after an elongation step. Δx_0 and Δy_0 describe the changes in length.

The stretch was calculated for increasing elongation values, but the initial distance (x_0/y_0) never changed. Only Δx_0 and Δy_0 increased their values and so other stretch values could be calculated. An example is given in subsection 3.1.4. In the same chapter the results are depicted. The diagrams show the relation between the local and global stretch in axial and circumferential direction.

2.3. Confocal reflection microscopy

To get another quantification method for collagen fibers, another option was tested. Jawerth et al. (2010) proposed a method for fiber-orientation and brightness in collagen networks with the help of confocal reflection microscopy. Artym and Matsumoto (2010) also describe how the confocal reflection microscopy technique can be used on fibrilar collagen. Brightman et al. (2000) investigated unstained 3D-matrices of type I collagen. They propose an excitation wavelength of 488 nm and analysed even the diameter of collagen fibrils with confocal reflection microscopy.

Confocal reflection microscopy uses back scattered and reflected light from the collagen fibers for the image acquisition. The difference in the refractive index of the collagen fiber and its surrounding is the key factor for generating image information (Artym and Matsumoto, 2010). The reflected photons have always the same wavelength as the emission wavelength. To record the signal only an optical band pass filter with a resonance frequency which has the same value as the excitation wavelength has to be added. So another advantage is that reflection microscopy can be collected during a fluorescence measurement. No additional changes in microscope are required. Immunolabelling or staining of

collagen is also not necessary. As mentioned by both papers, Jawerth et al. (2010); Artym and Matsumoto (2010), there is one big limitation: The brightness of the detected collagen fibers is depending on their orientation. Fibers with an angle of above $50°$ from the image plane are not detectable.

In order to verify the statements of the above-mentioned authors, four different reflection microscopy measurements were performed simultaneously with an autofluorescence measurement. Porcine media, adventitia and human samples treated with elastase and collagenase got tested:

- Firstly, the reflection image of a porcine media was performed with an excitation wavelength of 488 nm for confocal reflection microscopy and an excitation wavelength for the autofluorescence of 514 nm. 514 nm were chosen because of the previous results for collagen excitation obtained in section 2.2, since elastin fibers got also excited with smaller wavelengths and the collagen signal is innately weaker. Finally the images got compared and can be seen in subsection 3.2.1.

- Secondly, a porcine adventitia was investigated with the same settings. The results are shown in 3.2.2.

- Thirdly, the porcine sample was replaced by an human media sample. This sample was treated with elastase. Therefore in the recorded images the collagen is visible.

- Fourthly, a human media sample which was treated by collagenase was examined. The excitation wavelength for the autofluorescence of elastin was increased to 561 nm, according the results in section 2.2.

2.4. Multiphoton microscopy

The titanium-sapphire laser was used for the acquisition of the multiphoton microscopy images. This laser provides an excitation wavelength of 690 to 1040 nm, but was operated in the course of this master thesis exclusively with an excitation wavelength of 880 nm. With the laser beam, the effect of multiphoton excitation is used to induce the autofluorescence of collagen or elastin, respectively. The electrons of the corresponding proteins are excited by the simultaneous absorption of two or more photons. As a result, the electron is lifted into the excited state, remains there for a few nanoseconds and emits the characteristic autofluorescence wavelength of the protein when returning to the ground state (Denk and Strickler, 1990). The difference to the autofluorescence of confocal microscopy is that in normal fluorescence microscopy the excitation is performed by one single short-wave photon, whereas in multiphoton microscopy the excitation is conducted by two or more longer-wave photons at the same time. This has the advantage of a higher penetration depth.

To distinguish between collagen and elastin structures, a complex filtering system was used. The transmitted light from the investigated sample goes first through a short pass

filter (SP680, Leica Microsystems GmbH). Right after the light beam is split by dichroic mirror (95 DCXR, Leica Microsystems GmbH). This mirror allows a transmission of wavelengths between 300 and 485 nm and reflects light with wavelengths between 505 and 700 nm. The two beams are then each filtered by a bandpass. The first bandpass (BP460/50, Leica Microsystems GmbH) has cut-off frequencies of 435 and 485 nm, allowing photons emitted by collagen to pass through. The second bandpass (BP525/50, Leica Microsystems GmbH) allows light to pass through in the range of 500 to 550 nm. With this channel elastin gets detected. The necessity of the short-pass filter results from the characteristics of the bandpass filters. They perform excellently in the working range, but transmit radiation over a wavelength of 800 nm. To prevent this wavelengths from causing any artefacts, they get simply removed from the short pass filter. This filter allows only wavelengths under 680 nm to pass trough. Figure 3.17 shows on the left side the elastin signal and on the right side the collagen signal. As already mentioned the elastin signal is stronger than the collagen. Therefore, to get results like in Figure 3.17(b), the image obtained from elastin was always subtracted from the collagen image. This operation ensured that no elastin fibers were visible in the collagen images.

During the multiphoton microscopy imaging, two samples from a highly atherosclerotic abdominal aorta of an 80-year-old male person and one sample from a highly aneurysmatic abdominal aorta of an 81-year-old man got investigated. All three abdominal aortas are depicted in Figure 2.1. All data of the following measured and calculated parameters come from these three samples. Therefore, the changes in diameter, waviness and amplitude from the original unloaded state to high stretch values from elastin and collagen fibers are measured. For this purpose, the recorded images of each stretch value were analysed individually.

Additionally, the data obtained from the multiphoton microscopy images were evaluated statistically with two different methods. On the one hand the Mann-Whitney U test can be used to determine whether two independent variables originate from populations having the same distribution. On the other hand the Spearman rank correlation investigates if there is an association between two variables.

2.4.1. Cauchy stress vs. stretch diagram

In addition to the optical change, the Cauchy stress in axial and circumferential direction should of course also be measured in order to be able to create a Cauchy stress-stretch diagram. This allows statements to be made about the mechanical properties. The Cauchy stresses were calculated from the stretch ratios in axial (λ_{ax}) and circumferential (λ_{circ}) direction and their applied forces (F_{ax} and F_{circ}, respectively). Two of the four load cells delivered the value for one direction and the linear actuators showed the corresponding stretch value. With the undeformed specimen thickness T and the undeformed length L

over which the forces were applied, the formula for the Cauchy stress is, the same as described by Humphrey et al. (1990),

$$\sigma_{ax} = \frac{F_{ax}\lambda_{ax}}{T \cdot L} \qquad (2.3)$$

Because the tested sample has a square base area, the same formula results for the circumferential direction (Equation 2.4).

$$\sigma_{circ} = \frac{F_{circ}\lambda_{circ}}{T \cdot L} \qquad (2.4)$$

The corresponding diagrams for the three different samples are depicted in subsection 3.3.1. The data was imported from the biaxial machine into *Matlab* and then used to create the diagrams.

2.4.2. Diameter detection

To measure the diameter of different fibers the recorded multiphoton microscopy images got imported to *Matlab*. To measure the diameter of an individual fiber, circles with a diameter corresponding to the thickness of the fibers were inserted. For this it must be assumed that the thickness of the fiber corresponds to its diameter. This process is depicted in Figure 2.4. For every single stretch value five pictures got selected by hand out of the image stack. Out of these five images 25 different fiber diameters got analysed. Afterwards, the values of the diameters got saved and represented in a box-and-whisker plot (Figure 3.21 and Figure 3.22).
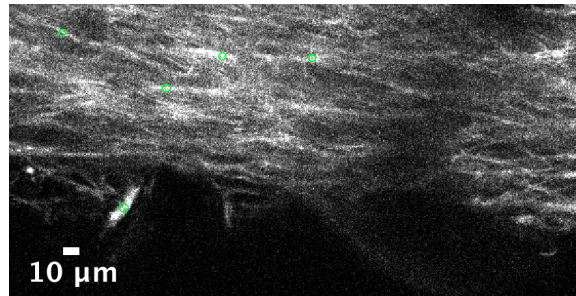
Figure 2.4   The picture shows five selected circles which are as big as the thickness of the fiber. The measured diameters represent the thickness of the fibers. This is an enlarged section of an multiphoton microscopy image of an elastin sample.

2.4.3. Tortuosity and amplitude detection

A further possibility for the analysis of collagen and elastin fibers is the quantification of waviness. In their basic state, both elastin and callagen fibers are not completely straight

Figure 2.5   The figure shows how the calculation of the paramters tortuosity and ampli-
             tude is performed. The rosa arch is designated as counter length, the blue line
             indicates the initial distance and the red line shows the height of the amplitude.

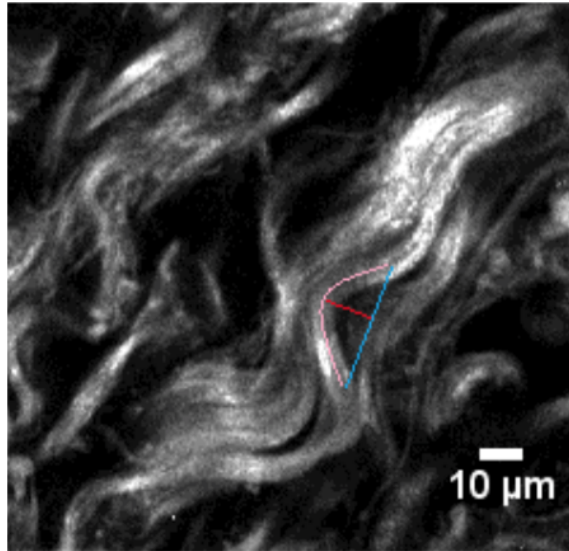in the tissue. In the unloaded state, collagen fibers show a certain waviness in order to
get stretched and work as main load carrying element. In order to be able to measure
the waviness, a method presented by Towler (2017) is used. To make the definition of
tortuosity and amplitude easier to explain, first have a look at Figure 2.5.

  The figure shows a collagen fiber and how it is measured. The length of the rosa arch,
designated as counter length (l_c), is measured by hand in the beginning with the plug-
in *NeuronJ* in *ImageJ*. Five of these arcs were then searched and measured per image.
Afterwards the measured data got imported to *Matlab*. In *Matlab* the initial distance (l_0) of
each arch was calculated. l_0. The blue line in Figure 2.5 indicates the initial distance. So
finally the tortuosity T is defined with

$$T = \frac{l_c}{l_0}. \tag{2.5}$$

But now it is possible that two different types of fibers with different waviness have the
same value for T, the amplitude is also determined. The amplitude is the red line in Fig-
ure 2.5 and refers to the height of the waviness of the fibers (Towler, 2017). This step
was repeated again for all stretch values and displayed in box-and-whisker plots in subsec-
tion 3.3.3.

2.4.4. Fiber Orientation

  In this part of the thesis the collagen and elastin fiber dispersion should be analysed. In
order to characterize the orientation, two parameters shall be presented first. The first one

is the mean fiber angle ϕ, also called the in-plane angle and is defined with $\phi \in [0, 2\pi]$. Expressed in degrees, an angle of $\phi = 0°$ represents an orientation in the circumferential direction. This means that the degree in axial direction can be calculated with $\phi_{ax} = 90° - \phi$ (Sherifova et al., 2019).

But the fibers can be dispersed in different ways. For example, many fibers may extend in one main direction or may be equally dispersed in the tissue. Therefore the scalar quantity κ_{ip} is introduced, which measures the in-plane dispersion of the fibers. It is defined with:

$$\kappa_{ip} = \frac{1}{2} - \frac{I_1(a)}{2I_0(a)} \tag{2.6}$$

where κ_{ip} is restricted by $0 < \kappa_{ip} < \frac{1}{2}$. a is a concentration parameter and determines the shape of the distribution. The concentration parameter a is based on the von Mises-distribution. The von Mises-distribution is similar to the normal distribution except it is used for periodic functions. I_0 and I_1 are the modified Bessel's function of order zero and one, respectively (Niestrawska et al., 2016; Sherifova et al., 2019; Schriefl et al., 2016).

On the one hand it can be said that if $a \to \infty$ means that $\kappa_{ip} \to 0$ and indicates that all of the fibers are perfectly aligned. On the other hand a value of $a \to 0$ signifies $\kappa_{ip} \to \frac{1}{2}$ and denotes that the fibers are equally dispersed. The calculation of κ_{ip} was performed in *Matlab* according to Niestrawska et al. (2016). The necessary data were obtained before with the plug-in *AngleExtraction ImageJ* which was implemented by Zehentner (2018). For each stretch level five pictures were selected. The plug-in creates also intensity plots of fiber orientation at different stretch values. The data got normalized and wedge filtered with a wedge with of $3°$. The results are depicted in subsection 3.3.4.

2.4.5. Statistical analysis

In this chapter, the previously recorded data on diameter, amplitude, tortousity, κ_{ip} and mean fiber angle ϕ are statistically analysed. Common features or strong distinctions between the measured values are to be recognized. The Mann-Whitney U test and Spearman rank correlation methods were used for this purpose. Both of the statistical methods are nonparametric tests. Nonparametric test are suitable for comparing two independent samples with not normally distributed outcome and the sample size is small (W. W. LaMorte., 2017). These three conditions are met for the data collected.

Mann-Whitney U Test

The Mann-Whitney U test, is a test which can be used to test if there are statistically significant differences between two populations. In this case, the Mann-Whitney U test is always performed as a two-sided test with two possible outcomes: an approval or rejection of the null hypothesis. The first one is $H = 0$ which means the two populations are equal and indicates that there is no statistical difference between both of them. The second one, $H = 1$, states that there is a statistical difference and therefore the populations are not

equal. The hypothesis is given below a significance of 5% (W. W. LaMorte., 2017). The analysis was performed in *Matlab*.

In order to obtain meaningful results, parameters of each human sample at a specific stretch level were compared with the same parameters at the subsequent stretch level. Thus it is possible to detect differences that occur due to a higher stretch value. For example, if the diameter only changes evenly up to a certain point, but then suddenly the diameter tapers rapidly, this becomes apparent because of the rejection of null hypothesis. The tables listed in section A.2 show the results of the Mann-Whitney U test. Each table shows the parameters for one human sample. The rows show the parameters which got investigated; the columns show the stretch levels compared. For example the column with the designation $6\,\%$ vs $8\,\%$ compares all measured values of one parameter at a stretch level of $6\,\%$ with all the values from the same parameter at 8%. A rejection of the null hypothesis is indicated with a $'1'$, $'0'$ stands for an approval of the null hypothesis.

The entire results of the Mann-Whitney U test are listed in the appendix. Table A.2 shows the result for the parameters of collagen in atherosclerotic tissue. Table A.3 and Table A.4 include the results for atherosclerotic elastin sample. Table A.5 shows the differences and similarities between the various parameters of a person with an abdominal atherosclerotic aneurysm. The results relating to the individual parameters can be found in the respective chapter.

Spearman Rank Correlation

Spearman rank correlation is used to test the association between two independent variables. It indicates if their is a linear or non-linear relationship between the two variables. It is possible to use as long as the variables are monotonic. In contrast to the linear regression the Spearman rank correlation is based on the ranks of the variables. For the calculation both variables get ranked according their value. The Spearman rank correlation coefficient, ρ, can get values from $[-1, 1]$. A value of $\rho = 0$ indicates that there is no covariance between the two ranks of the variables, $\rho = 1$ means that the ranks are perfectly monotonically related. If one variable tends to increase and the other tends to decrease, the result is a negative ρ-value (J. H. McDonald., 2015). Additionally to the correlation coefficient, the p-value was calculated. A small p-value ($p < 0.05$) means the correlated ρ is significantly different from zero. Higher p-values indicate that there is no correlation.

The calculation was again performed in *Matlab*. The median values of the different parameters were used to calculate the Spearman correlation. The sample number of every parameter is five (n = 5). In conclusion, it can be said that in this analysis the median values of diameter, amplitude, tortuosity, κ_{ip} and ϕ are ranked for each stretch level in order to be able to check their correlation. The results of all test are in tables in the appendix A.3. Table A.6, Table A.7 and Table A.8 show compared parameters of atherosclerotic elastin and collagen fibers, respectively. Table A.9 concludes with the results of the correlation of an aneurysmatic sample. Statistical abnormalities of the individual parameters can be found again in the corresponding chapter.

3. Results

This chapter shows the results of confocal microscopy, reflection microscopy and multi-photon microscopy of porcine and human samples as well as the performed biaxial extension tests. The photographs acquired during the microscopical examination are depicted and the associated plots are integrated. Furthermore all Cauchy stress-stretch plots, box and whiskers plots, and calculations can be found in this chapter.

3.1. Confocal microscopy

3.1.1. Autofluorescence of porcine sample

This section shows the different autofluorescence results which were obtained by the different excitation wavelengths. The following pictures show the difference between various excitation wavelengths. Figure 3.1(a) was excited with 488 and 561 nm simultaneously. In Figure 3.1(b), three different wavelengths (458, 476 and 561 nm) were used. It turned out that the autofluorescence of the two proteins can be achieved with different excitation wavelengths. A combination of several wavelengths leads to higher autofluorescence intensity.

All other excitation wavelengths and combinations of different wavelengths did not result in any satisfying result. Therefore, none of them are depicted in this thesis. As a result of this test, it can be seen that no distinction between collagen and elastin can be made by changing the excitation wavelength.

3.1.2. Autofluorescence of human sample

Figure 3.2 depicts human media sample treated with collagenase. The images are compared which were taken by different excitation wavelengths. The position of the sample has not been changed during the test, which means in every picture the same spot is depicted.

The direct comparison of these four images clearly shows that the best autofluorescence of human elastin tissue occurs at an excitation wavelength of 561 nm, depicted in Figure 3.2(c).

The results from Figure 3.2 led to an excitation wavelength of 561 nm during the performance of the lambda scan. The emission spectrum of elastin can be found in Figure 3.3. The same procedure was used to find the optimal excitation wavelength for collagen. It

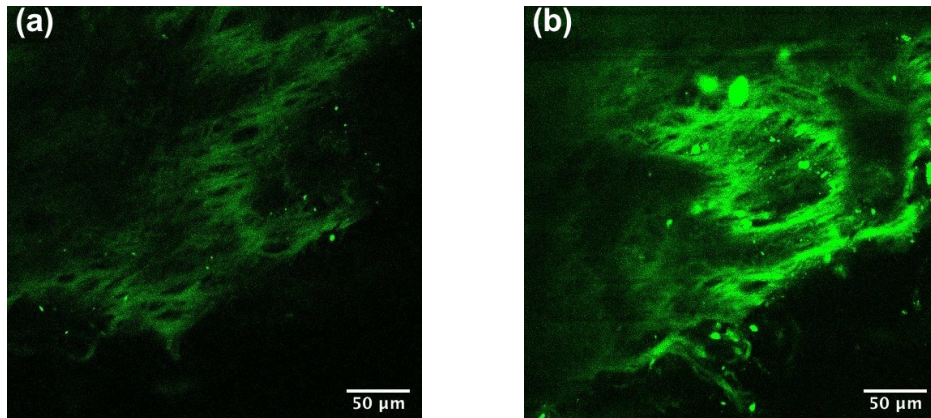Figure 3.1   Autofluorescence microscopy of an porcine media sample. The images were
             acquired with an excitation-wavelength of **(a)** 488 and 561 nm and **(b)** 458,
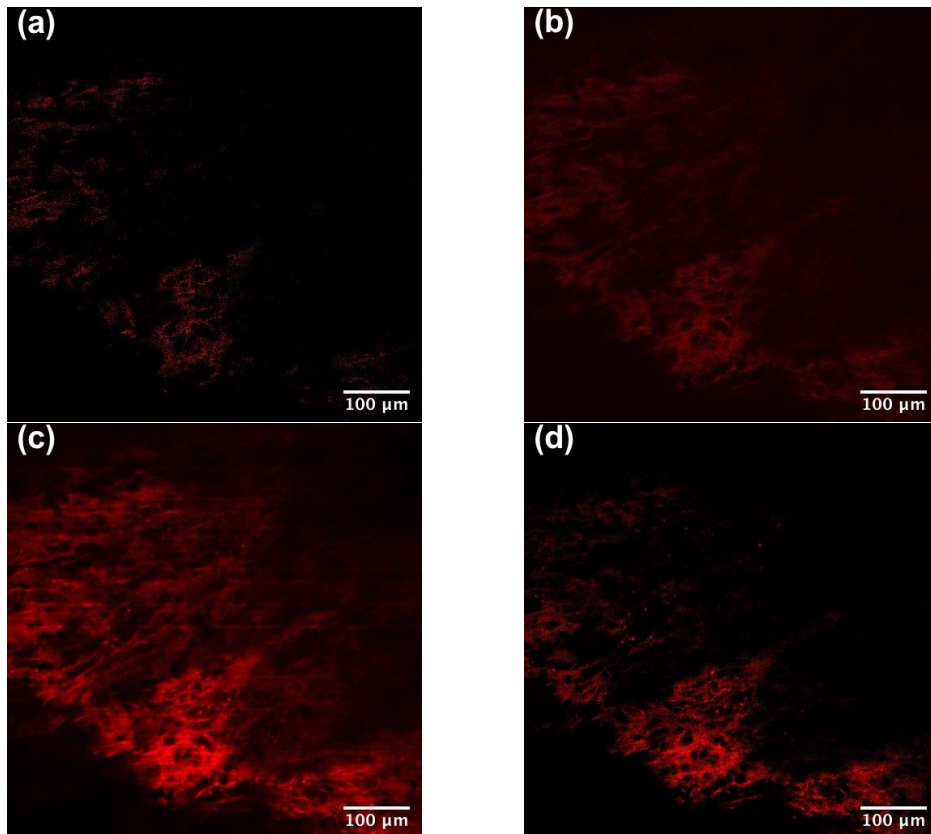   476 and 561 nm on the same spot of the porcine sample
             .

Figure 3.2   Elastin-only sample of a human media excited with **(a)**: 458 nm, **(b)**: 514 nm,
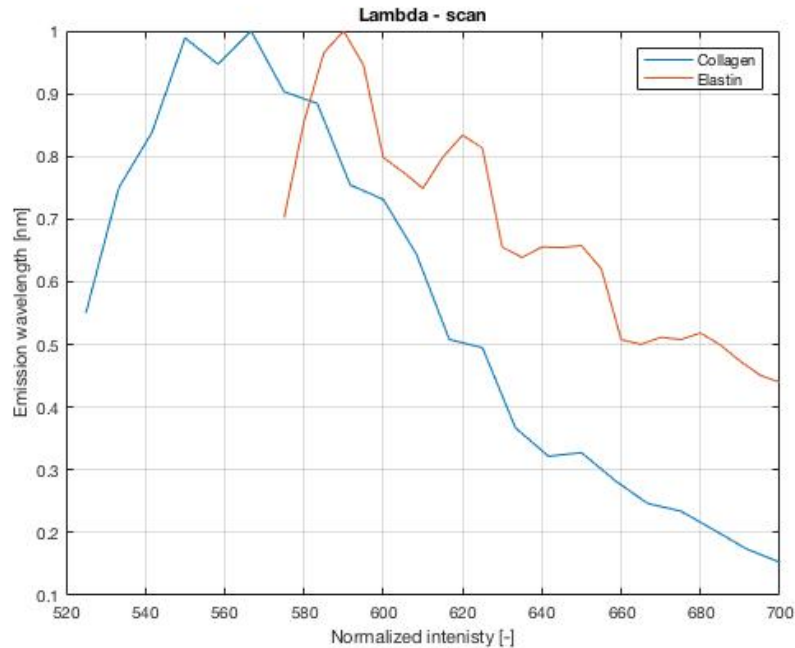   **(c)**: 561 nm and **(d)**: 633 nm. (Person #1)

Figure 3.3   The results of the lambda-scan of a collagen and elastin sample with emission maxima at 567 nm and 590 nm, respectively.

turned out that the the ideal excitation wavelength is 514 nm. At this wavelength the result of the recordings was clearly the best. Figure 3.3 also shows the emission spectrum of collagen.

The results were used to adjust the settings for the following tasks. The tests showed that the ideal setting for the *Leica SP5* with the possible excitation wavelengths are for **Elastin**:

- Excitation wavelength: 561 nm,

- Emission maxima: 590 nm,

and for **Collagen:**

- Excitation wavelength: 514 nm,

- Emission maxima: 567 nm.

3.1.3. Intensity of elastin and collagen autofluorescence

The images in Figure 3.4 show the different images which were recorded with a photon counting imaging technique. The pictures show collagenase treated human media. In Table 3.1 and Table 3.2 Figure 3.4(a) is referenced as *AC1*, Figure 3.4(b) as *AC2*, and
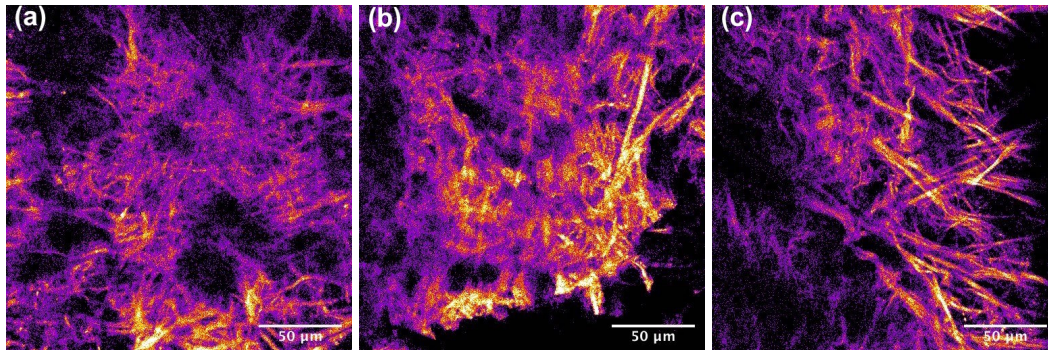
Figure 3.4   Images recorded from photon-count measurement on an elastin-only sample. **(a), (b)** and **(c)** are representing different spots on the same sample. (Person #1)
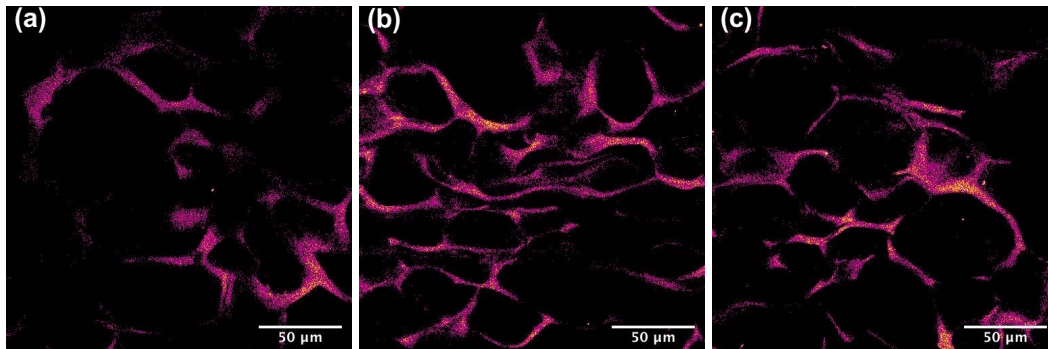

Figure 3.5   Images recorded from Photon-count measurement and representing collagen-only samples. Also here the pictures **(a), (b)** and **(c)** describe different places on the same sample. (Person #1)

Figure 3.4(c) as *AC3*. These pictures are presented in another colour scheme to make the difference in intensity better visible. The bright/yellow spots show a higher amount of photons in that specific spot on the sample. The dark/violet areas in the picture indicate only a small amount of photons.

Figure 3.5 shows the same as mentioned above for an elastase-treated human media. In the following two tables data recorded from Figure 3.5(a) are called *AE1*, from Figure 3.5(b) *AE2* and from Figure 3.5(c) *AE3*.

Table 3.1 represents the data which were derived by the measurement of the fluorescence background readings. Therefore areas from Figure 3.4 and Figure 3.5 with no fluorescence were measured. The *Area* values are given in square pixels. All calculations were performed in *pixel* so that a conversion to *μm* did not have to take place in every step. Besides, the final result is a value with an optical quantity. It is the *Mean Gray Value* and a dimension-less quantity, which only shows how bright one pixel actually is.

Table 3.1 Mean fluorescence of background readings

Background Emission	Area [px^2]	Mean Gray Value [-]
BG_AC1	1025	0.3586
BG_AC2	633	0.3724
BG_AC3	518	0.3381
BG_AE1	1040	0.0015
BG_AE2	980	0.0019
BG_AE3	544	0.0021

In Table 3.2 the number behind the name of the sample indicates another measuring point within the same image. *Area* is given in square pixel again. *Integrated Density* and *BCTF* is dimensionless. To calculate the value of *BCTF* Equation 2.1 was used. The following example takes a closer look to the values of *AC1*. For the calculation of the *BCTF*, one takes the *Integrated Density* of a specific spot on one sample from Table 3.2. Afterwards, the corresponding *MGV* of background emission from Table 3.1 had to be multiplied with the selected area in the same table:

$$BCTF = IntDen(AC1.1) - Area(BG\_AC1) \cdot MGV(BG\_AC1)$$
$$= 146 - 35[px] \cdot 0.3586[px^{-1}] \approx 134[-]$$

(3.1)

The calculation was repeated for always two different spots on each sample. To get a better overview, the total amount of the *BCTF* is presented in a diagram in Figure 3.6. The result shows a significantly higher intensity of autofluorescence of elastin compared to collagen.

The box and whisker plot in Figure 3.7 show on the left side, that the elastin tissue is capable of an average emission of 1.38 photons per pixel. The mean emission of the collagen tissue is limited to 1.09 photons per pixel. This confirms the previous calculations that elastin is able to generate a higher intensity of autofluorescence. The box and whisker plot of collagen is just a vertical line because most of the photon-value per pixel was 1 and the maximum was a photon count of 2.

3.1.4. Analysis of local and global stretch

In Figure 3.8 the microspheres on the sample are presented. The microspheres are penetrating the tissue. Both images were created by superimposing a stack of images from one elongation step. This process was necessary to be able to scan all reference points in the medium on one image. When the tissue is stretched thus also the position of every microsphere changes. This can be seen very well by comparing the image at the initial position (Figure 3.8(a)) with the image taken at maximal elongation (Figure 3.8(b)). With the help

Table 3.2   Background corrected total fluorescence and values which are needed for the
             calibration

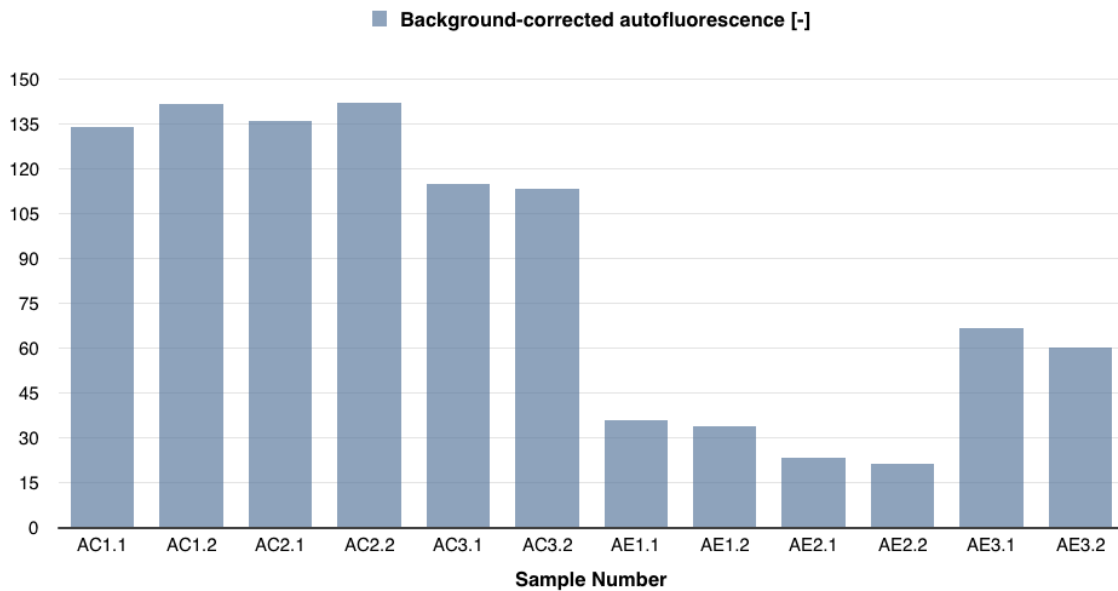| Sample	Area $[px^2]$	Integrated Density [-]	BCTF [-]
AC1.1	35	146	134
AC1.2	49	160	142
AC2.1	37	150	136
AC2.2	45	159	142
AC3.1	45	130	115
AC3.2	54	132	114
AE1.1	45	36	36
AE1.2	55	34	34
AE2.1	35	24	23
AE2.2	22	21	21
AE3.1	42	67	67
AE3.2	39	60	60

Figure 3.6   Comparison of Autofluorescence intensity. The first six bars represent the
              intensity of elastin, which is up to approximately 50% higher than collagen.
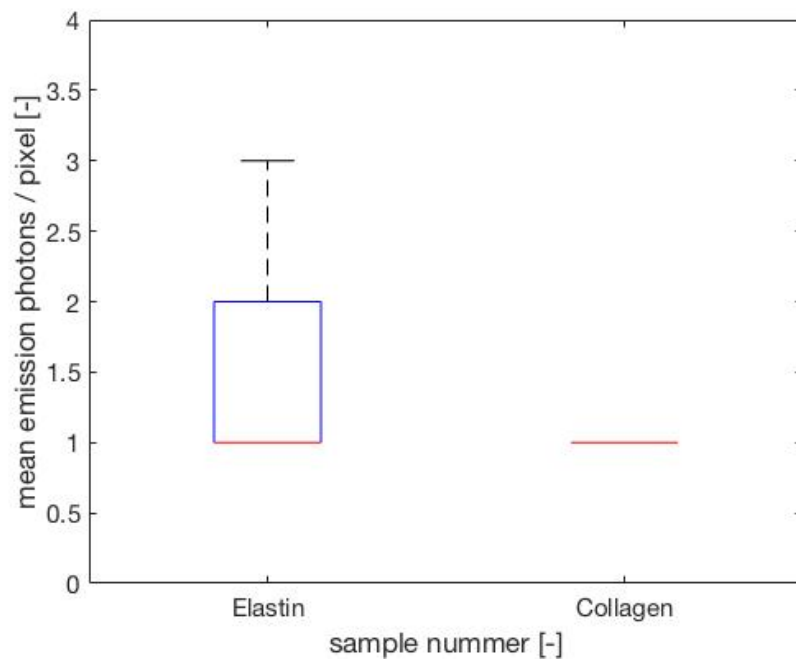   The results got background corrected.

Figure 3.7   Box and whsiker plot of elastin- and collagen-emission. Shown in average emission photons per pixel.
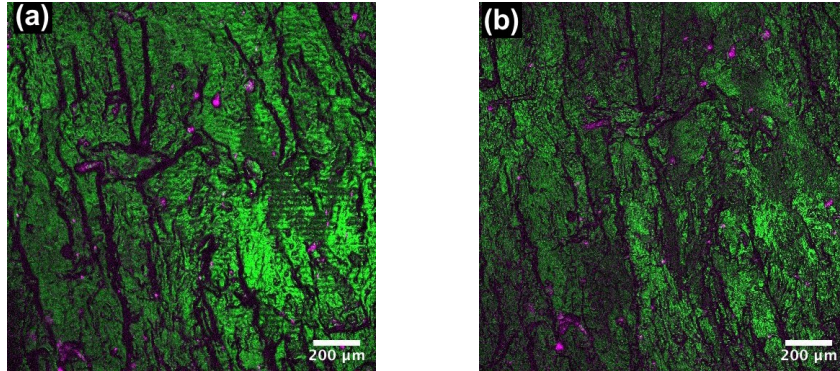
Figure 3.8   **(a)** shows the initial position of the microspheres without a global stress. **(b)**
on the contrary, shows the change in position of the microspheres at a global
stress of $12\,\%$. The images were created by superimposing all the images from
an image stack.

of these microspheres as reference points it is possible to calculate the local stress in the
middle of the tissue. All data recorded for the position of the microspheres can be found in
the appendix in Table A.1.

To calculate the local stretch in the sample Equation 2.2 was used. At this point a con-
crete example shall be given, microspheres *B3* and *B5* from Table A.1 will be considered.
The center of the microspheres in the unloaded condition are for

- $B3(222px, 204px)$

and for

- $B5(65px/378px)$

To get the initial distances between the two beads in horizontal and vertical direction the
coordinates has to be subtracted. The results are: $x_0 = 157; y_0 = 174$. After an elongation
of $2\,\%$ the new pixel values are for

- $B3(256px, 178px)$

and for

- $B5(96px/354px)$

To determine Δx and Δy, the coordinates got subtracted again and x_0 and y_0 has to be
subtracted too. This results in $\Delta x = 3$ and $\Delta y = 2$. Inserted into Equation 2.2 delivers the
stretch value:

$$\lambda_x = \frac{x_0 + \Delta x_0}{x_0} = \frac{157 + 3}{157} = 1.0191$$

$$\lambda_y = \frac{y_0 + \Delta y_0}{y_0} = \frac{174 + 2}{174} = 1.0115$$
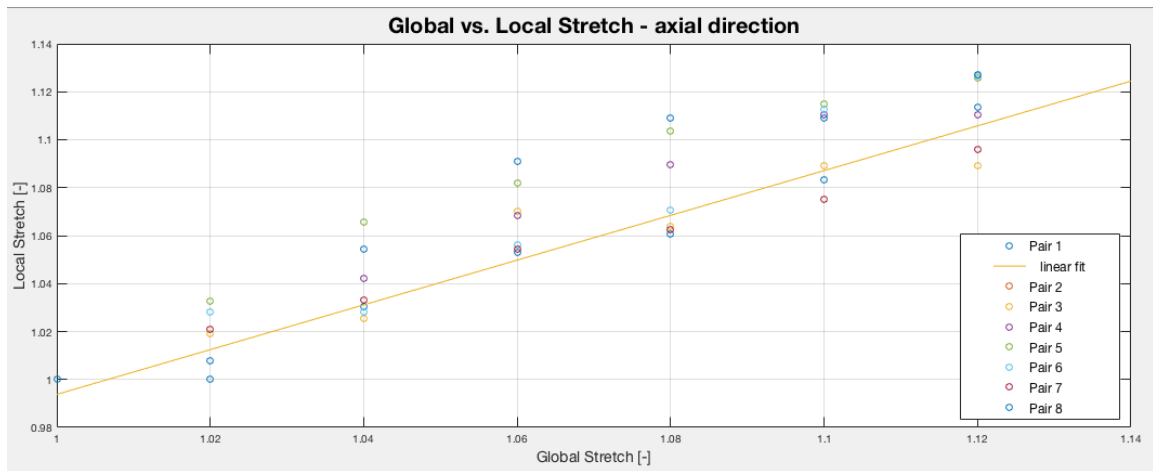
Figure 3.9   Comparison of local and global stretch values. The yellow line shows the linear regression of all data in axial direction.

According to the calculation of these two reference points, a global stretch of 2% results in a local stretch of 1.91% in axial direction and 1.15% in circumferential direction, respectively. The same calculation was now repeated for all other data points from Table A.1. Then all calculated values in axial and circumferential direction were inserted into two diagrams. Figure 3.9 shows the relationship of local and global stretch in axial direction of the sample whereas Figure 3.10 represents the same in circumferential direction. The results show an almost identical course of local and global stretch in the circumferential direction. Also in axial direction the local value is just slightly below the global stretch value.
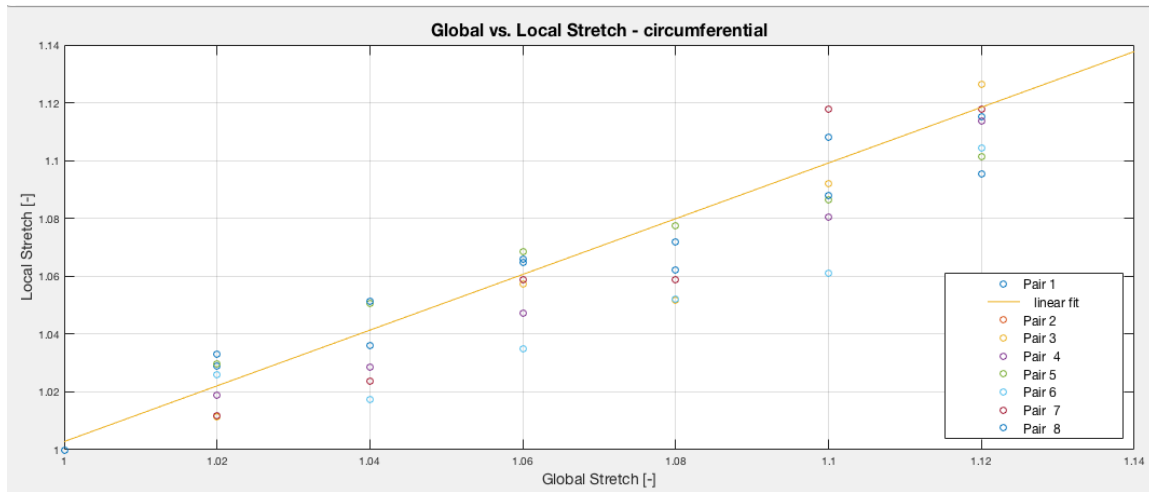
Figure 3.10   Comparison of local and global stretch values in circumferential direction. The yellow line again represents the linear fit of the data.

3.2. Confocal reflection microscopy

This section compares reflection microscopy images and confocal microscopy images of different tissues. In the beginning, the two individual images of reflection microscopy and the autofluorescence image are presented. The reflection microscope image is always coloured in red. In contrast the autofluorescence picture is coloured in green. Afterwards, there is always a merged image so that the two visible structures can be compared with each other.

3.2.1. Porcine media sample

In Figure 3.11(a) the reflection autofluorescence microscopy of an porcine media sample is illustrated. Figure 3.11(b) shows the same tissue, but it was excited with 514 nm to get the autofluorescence signal. In Figure 3.11(c) the aforementioned images were superimposed to make a comparison possible. It is noticeable that the reflection microscopy image shows more of the collagen structure from the porcine arterial wall.
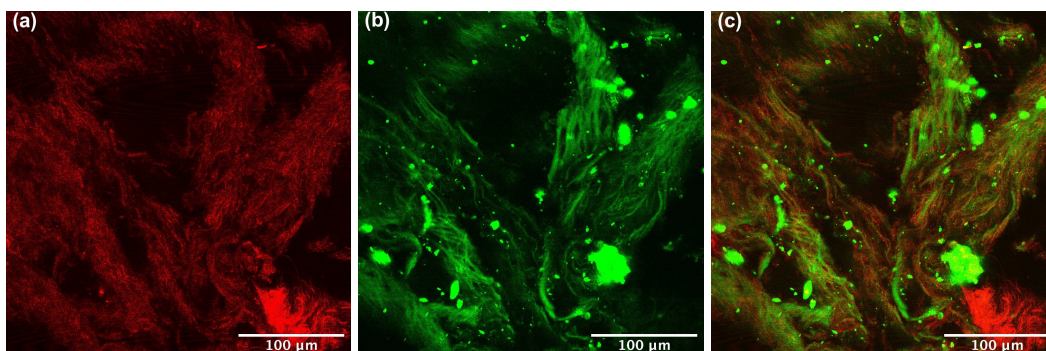
Figure 3.11 **(a)** shows the reflection microscopy image and **(b)** the autofluorescence image of the same spot on an porcine media sample. **(c)** is the superimposed image of (a) and (b).

3.2.2. Porcine adventitia sample

The results from the porcine adventitia sample show also very distinct the difference between the two different microscopy methods (Figure 3.12(a) and (b)). More of the waviness structure of the tissue, which could indicate the collagen fibers, are better visible in the reflection microscopy image. However, the structure as a whole can best be assessed in the merged image in Figure 3.12(c).
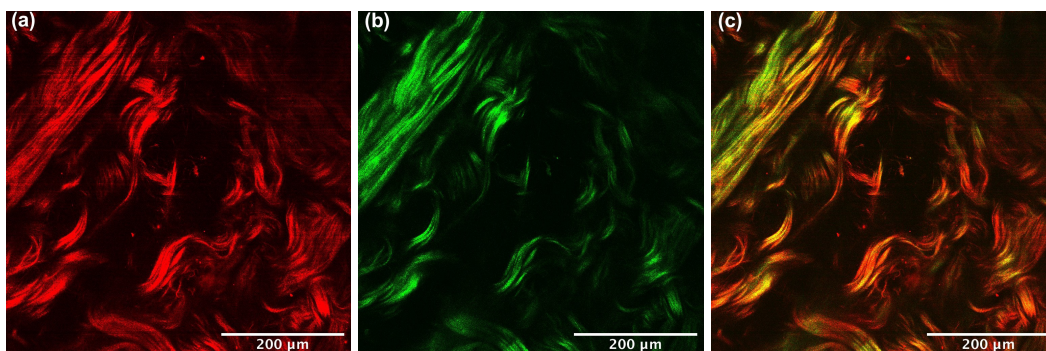
Figure 3.12 The reflection microscopy **(a)** and autofluorescence image **(b)** of a porcine adventitia. In the merged picture **(c)** the strucutre of the adventitial collagen is clearly noticeable.

3.2.3. Human media sample treated with elastase

The results of a collagen-only human tissue are present in this part of the thesis. For a better comparison to the results a bright field picture of a media treated with elastase

is shown in Figure 3.13. Figure 3.14 shows a similar structure for the collagen tissue. Figure 3.14(a) is representing the reflection microscopy image of the collagen structure of an human media after elastase treatment. Figure 3.14(b) illustrates the autofluorescence of the same sample spot. Figure 3.14(c) was taken to make the differences visible.
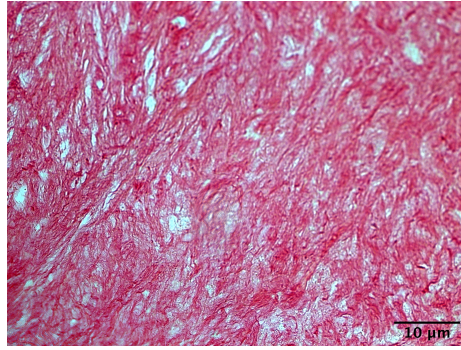
Figure 3.13   Brightfield microscopy of an human media treated with elastase
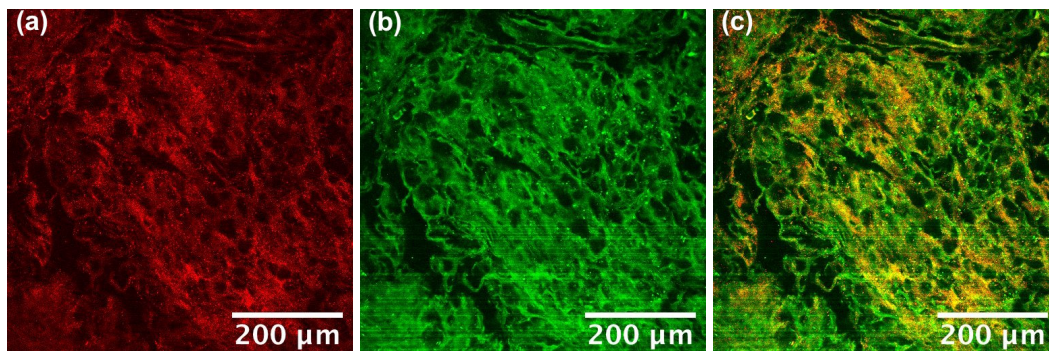
Figure 3.14   **(a)** shows the reflection microscopy of a human media sample treated with elastase; **(b)** depicts the same sample but just the autofluorescence signal; **(c)** is the superimposition of **(a)** and **(b)** to compare the imaging techniques. (Person #1)

3.2.4. Human media sample treated with collagenase

In the end a tissue treated with collagenase is examined. Figure 3.15 shows a brightfield image of the same tissue. Figure 3.16(a) proves that elastin does not generate a reflection microscopy image. Therefore the difference between the autofluorescene image of elastin in Figure 3.16(b) and the merged image in Figure 3.16(c) is minimal.
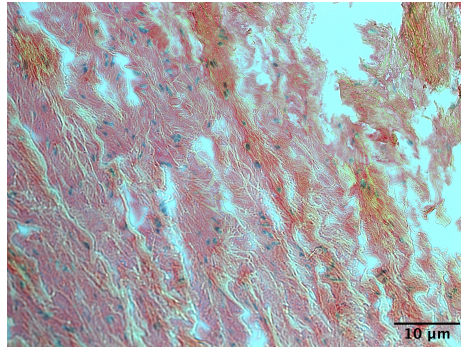
Figure 3.15   Brightfield microscopy of an human media treated with collagenase
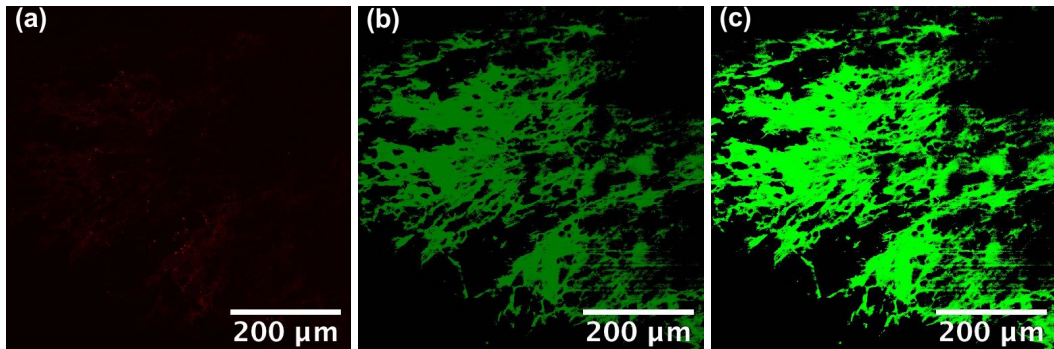
Figure 3.16   Elastin structure of an human media recorded with reflection microscopy technique (a) and with autofluorescence microscopy (b). The merged picture in (c) is nearly identical with the autofluorescence image, since the reflection microscopy image does not generate an image for elastin tissue. (Person #1)
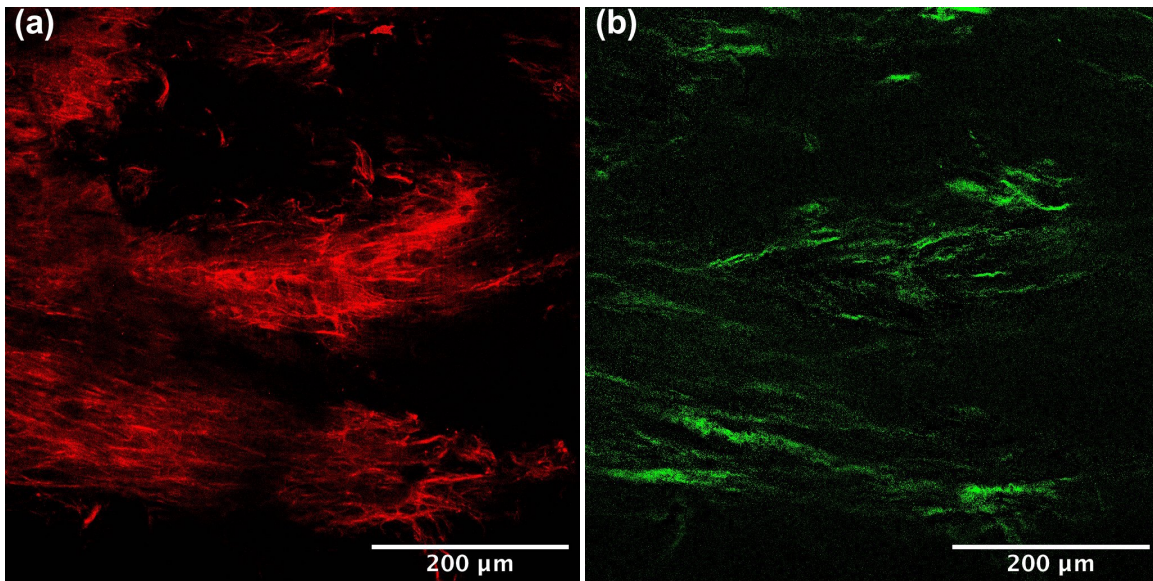
Figure 3.17   Multiphoton microscopy image of elastin fibers **(a)** and collagen fibers **(b)**.
(Person #3, Sample 1)

3.3. Multiphoton microscopy

This section provides all the results which were obtained by the means of a multiphoton microscopy image. Figure 3.17(a) shows the image which was acquired by the elastin signal. Figure 3.17(b) displays the image from the collagen signal. The multiphoton microscopy image depicts a human atherosclerotic artery at a stretch level of $10\,\%$. With the help of such images all further parameters were measured and calculated, respectively.

3.3.1. Cauchy stress vs. stretch diagram

The Cauchy stress-stretch relations in the following figures provide information about the elasticity and stiffness of the tested material. In Figure 3.18 the atherosclerotic sample of an aortic media tissue got investigated. After the pre-conditioning the stretch was increased in 0.02 increments up to a value of 1.3.
The aortic atherosclerotic media sample used to represent the diagram in Figure 3.19 was also performed with a 0.02 increment. Due to the composition of the sample, the data could only be recorded up to a stretch of 1.18.
The last sample was taken from a male patient with abdominal atherosclerotic aneurysm. The test could be performed up to a stretch of 1.3 with a 0.02 increment again and is depicted in Figure 3.20.
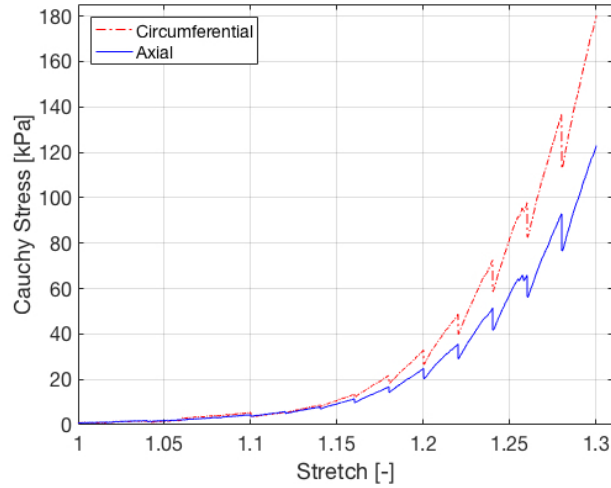
Figure 3.18   Cauchy stress vs. stretch-diagram of an human abdominal aortic media sample of an 80-year-old male person with a high level of atheroscleroses. (Person #3, Sample 1)
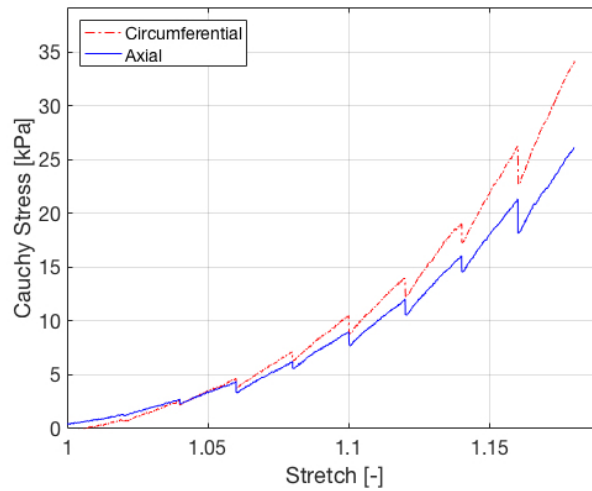
Figure 3.19   Cauchy stress vs. stretch-diagram of the same person as in Figure 3.18. This media sample was taken from another spot of the abdominal aorta. (Person #3, Sample 2)
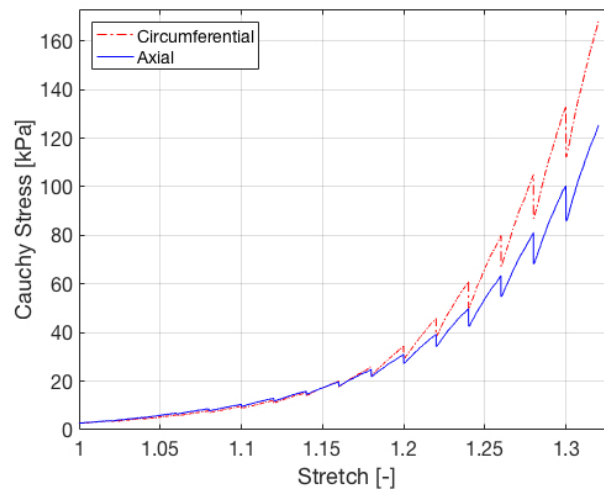
Figure 3.20   Cauchy stress vs. stretch diagram of an human abdominal aortic media
sample of an 81-year-old male person with an abdominal atherosclerotic
aneurysm. (Person #2)

3.3.2. Diameter detection

Here, too, the same three tissue samples as in the previous chapter were recorded. For
the first sample of the severely atherosclerotic tissue a two-channel image was obtained
as planned. The two channels show the elastic fibers and the collagen fibers. The results
from the diameter measurement are shown in Figure 3.21. On the left side the diameter
of collagen fibers can be seen which diminishes from an initial mean diameter of 8 μm to
final mean of 3 μm. The elastin diameter shows a more straight course and starts with a
mean diameter of 4.6 μm and ends at around 3.6 μm. Looking at these diagrams, the strong
fluctuation of the median value is noticeable. The measured images have a resolution of
0.57μm/pixel. The measured diameters have a maximum value of 10μm. This explains the
high fluctuation range.
 The elastin diameter quantification of the second atherosclerotic tissue (*Person #3, Sample
2)* is on the left side, the sample with an abdominal atherosclerotic aneurysm *(Person #2)*
is shown on the right side of Figure 3.22.
Height and course of the diameter of elastin show similar results as in Figure 3.21. The
Mann-Whitney test of the first atherosclerotic sample shows a statistical difference for eval-
uation of elastin and collagen diameter at the spots of 6 % vs 8 % and 16 % vs 18 %. There
is no statistical significant change in the second atherosclerotic tissue. The aneurysmatic
samples features a change at 22 % vs 24 %. The Spearman rank correlation tests show a
strong monotonic relation between diameter and amplitude as well as diameter and tortu-
osity for all samples. The other parameters got rejected because the $p-$value is to high or
the correlation is minimal.
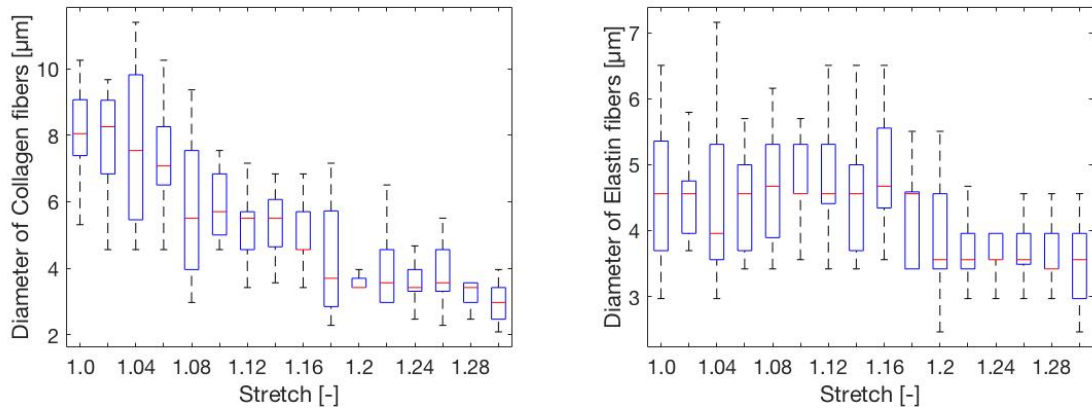
Figure 3.21   Quantification of collagen-diameter on the left side and elastin-diameter on the right side. Both proteins show a decreasing trend in diameter of the atherosclerotic tissue. (Person #3, Sample 1)

For the two samples of *Person #1, Sample 2* and *Person #1*, however, only the channel that recorded the elastin wavelength achieved satisfactory results. The possible reasons why a successful collagen signal could not be recorded can be found in section 4.3.
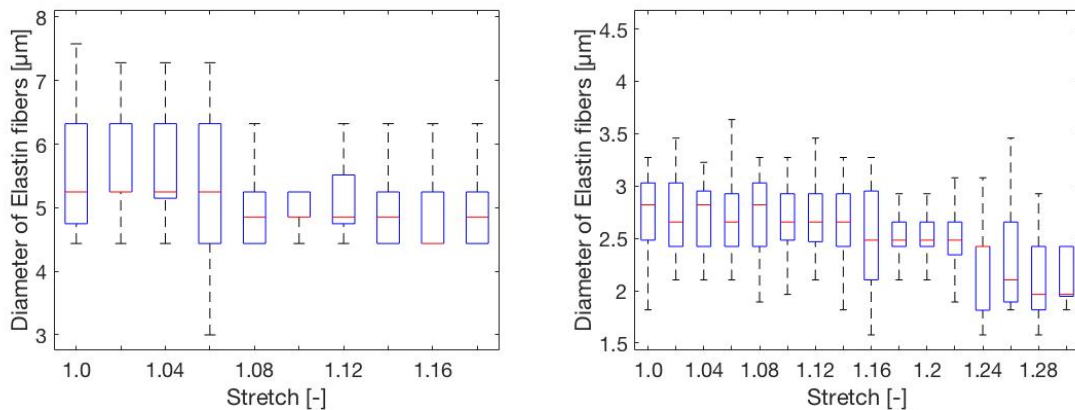
Figure 3.22   Both diagrams show the diameter progression of elastin fibers. On the left
               side an atherosclerotic tissue got investigated (Person #3, Sample 2). The
               right side shows the evaluation of the diameter in a sample with an abdominal
               aortic aneurysm. (Person #2)

3.3.3. Tortuosity and amplitude detection

As can be seen Figure 3.23 the average value of elastin fibers in atherosclerotic tissue is
decreasing fast in the beginning with increasing stretch. The tortuosity, on the other hand,
shows a very low decrease from a value of 1.05 to 1.01. The decrease of the amplitude of
collagen in atherosclerotic tissue in Figure 3.24 can be described as approximately linear.
In contrast to elastin, the amplitude is higher. There is still only a minimal decrease in tor-
tousity, but it is again higher compared to elastin. When analyzing the data, the fluctuation
range due to the resolution must also be taken into account here. The elastin amplitude and
tortuosity in Figure 3.25 both show a very smooth decrease of its values. The amplitude
is little bit higher compared to the other atherosclerotic elastin tissues. It is noticeable that
the final value of the tortuosity is almost 1. This indicates a very linear structure. The
diagrams of the aneurysmatic samples in Figure 3.26 show both a sudden sharp decrease
in the values at 10% stretch. Since the tissue is aneurysmatic, this may be due to a greater
structural change due to the extension of it.
The Mann-Whitney U test for atherosclerotic collagen start with indicating differences in
amplitude and tortuosity at 20% vs 22%. The results for amplitude and tortuosity of elastin
fibers are very similar. They are all equal at the beginning, but they start to differ a lot at a
certain point.
As already mentioned in the section before, the Spearman rank correlation shows a strong
monotonic relation between amplitude and diameter, amplitude and tortuosity as well as
tortuosity and diameter.
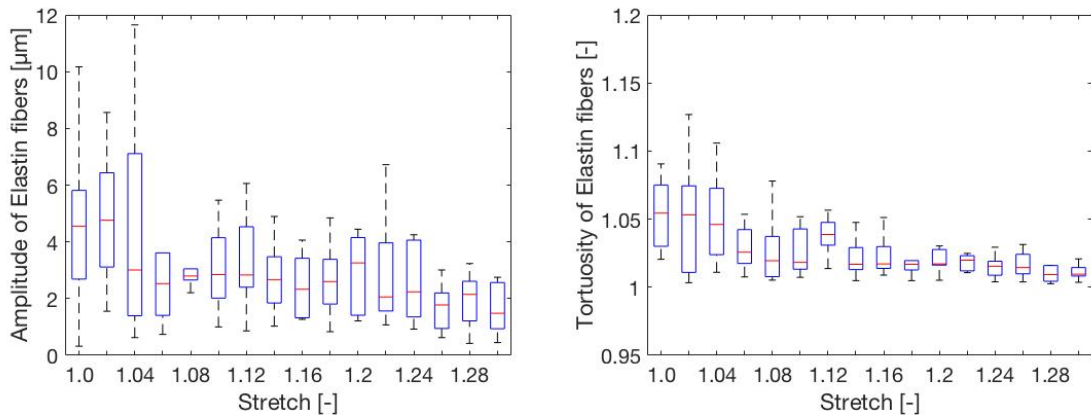
Figure 3.23   The diagrams show the course of elastin amplitude and tortuosity of an atherosclerotic aorta meadia sample. (Person #3, Sample 1)
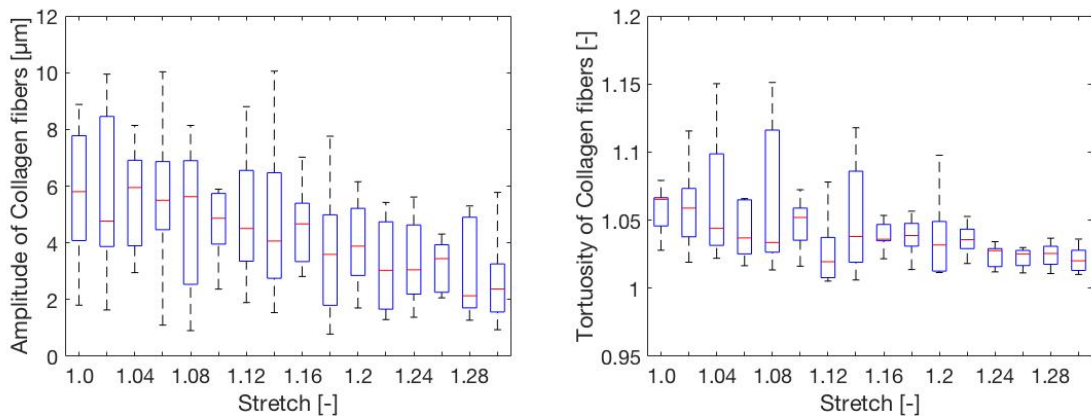
Figure 3.24   Collagen amplitude and tortuosity of atherosclerotic aortic media tissue. (Person #3, Sample 1)
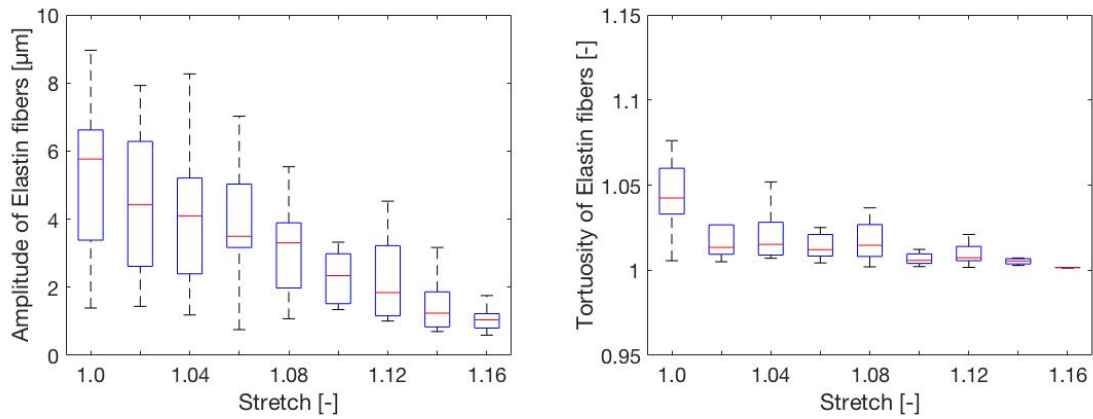
Figure 3.25   The diagrams show the course of elastin amplitude and tortuosity of an
               atherosclerotic media sample. (Person #3, Sample 2)
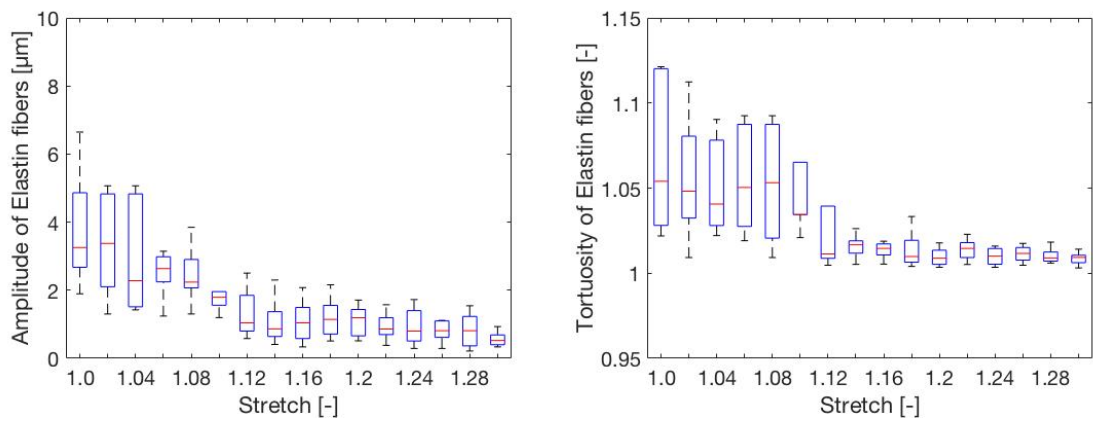
Figure 3.26   Development of the amplitude and tortuosity of an abdominal atherosclerotic
               aneurysmatic media tissue with increasing stretch. (Person #2)

3.3.4. Fiber orientation

The following intensity plots show the collagen and elastin fiber direction and orientation through different values of stretch level. The number of fibers which align in a specific direction are normalized (Figure 3.27). The intensity plots provide the same information as the tables in section A.4. A warm color scheme indicates that most of the fibers are aligned in one specific angle, whereas cool colors signify that there are only few or none fibers. The $0°$ mark in the middle of each plot corresponds to circumferential direction.
 As can be seen in Figure 3.28(a) elastin fibers seems to be better aligned in circumferential

Figure 3.27   Normalized number of fibers. Red *(1)* depicts no dispersion and blue *(0)* relates to no fibers under this angle.

direction than collagen (b). Both samples show that with increasing stretch the dispersion decreases. The sample depicted is atherosclerotic. The elastin of atherosclerotic human media in Figure 3.29 shows a large dispersion in the range of $-45°$ to $0°$ at a stretch level of 0%. The tissue becomes less dipersed with increasing stretch. The aneurysmatic tissue in Figure 3.30 displays strong dispersed fibers in the beginning , but with increasing stretch it aligns in the direction of $-16°$ degrees. The values of ϕ and κ_{ip} can be found in the appendix A.4.

The Mann-Whitney test for the parameters ϕ and κ_{ip} of collagen in the atherosclerotic sample state that all the changes are equal. The first atherosclerotic elastin sample only indicates one change at 14 % vs 16 % for κ_{ip}. The second one shows changes for ϕ and κ_{ip} at the last two measured positions. The dispersion coefficient κ_{ip} for elastin from the aneurysmatic tissue displays changes at almost every position, whereas the fiber angle is just at the spot of 14 % vs 16 % not equal. The Spearman rank correlation tests have little in common. Most of the values have to be rejected because of the high $p-$value or show a very low correlation.
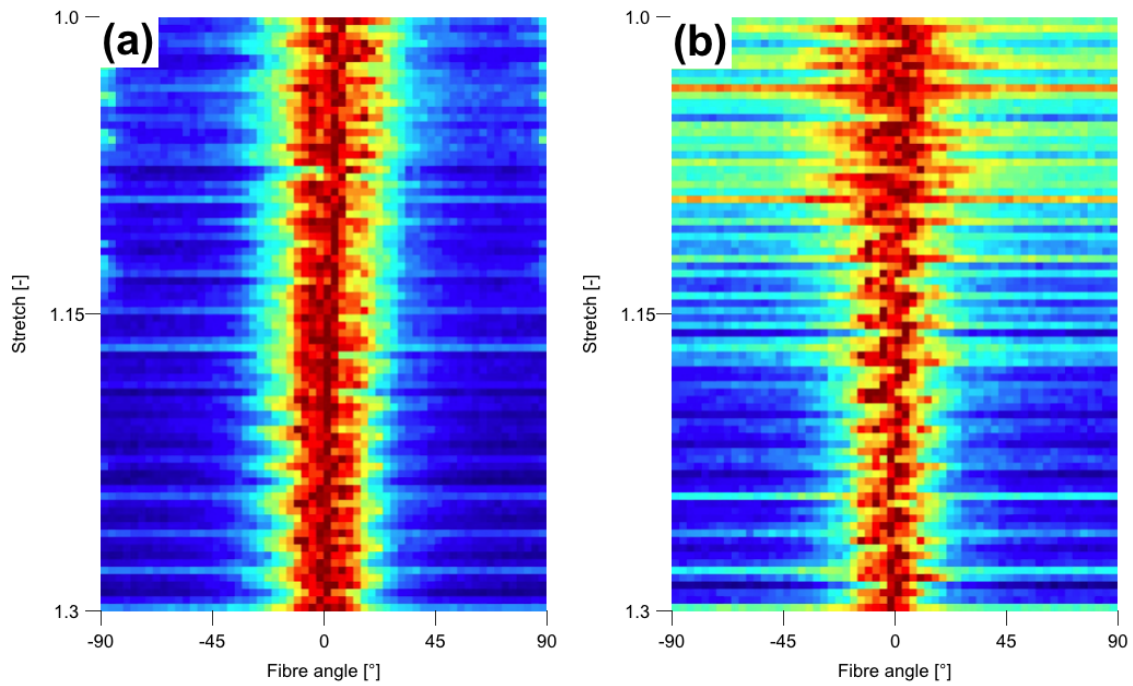
Figure 3.28   The left hand side shows the development of fiber dispersion of elastin **(a)** whereas the right hand side depicts the dispersion of collagen fibers **(b)** of an atherosclerotic human media sample. (Person #3, Sample 1)
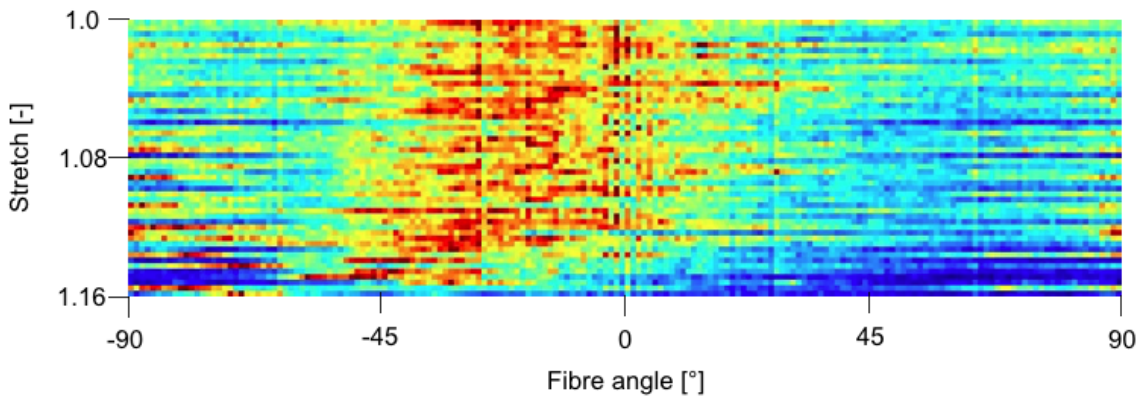
Figure 3.29   Intensity plot showing elastin fiber direction of an atherosclerotic human media. To obtain better results, the wedge width of the filter war reduced just for this plot to $1°$. (Person #3, Sample 2)
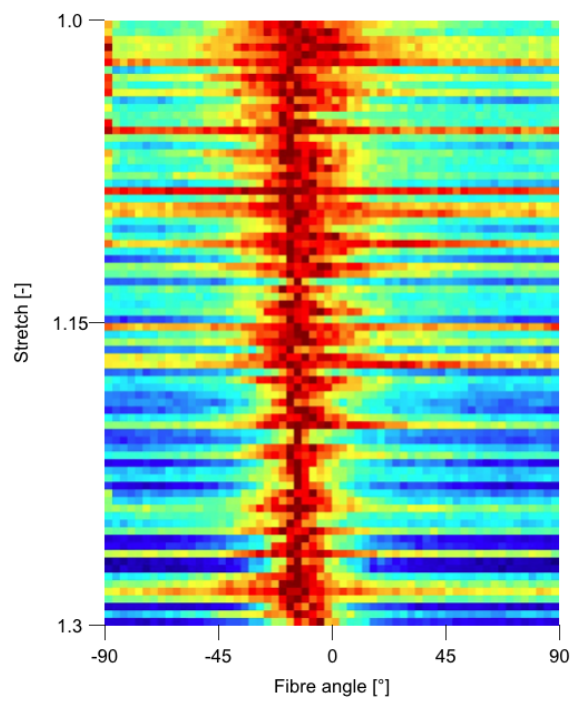
Figure 3.30   Intensity plot showing elastin fiber direction of an aneurysmatic human media. (Person #2)

4. Discussion

At this point, the most important observations from the results are summarized. The first part deals with finding the right settings for confocal microscopy for arterial tissue. This is necessary in to differentiate between the elastin and collagen emission spectrum in the further course of the project. First, the optimal excitation and emission settings for the autofluorescence of porcine samples had to be found. Second, the porcine sample was replaced by human aortic tissue. The human tissue was treated with collagenase and elastase to find precise settings for collagen and elastin. In the third step, the intensities of autofluorescence were compared in order to investigate further differentiation between elastin and collagen. The second part focused on confocal reflection microscopy. The third part concerns multiphoton microscopy. With the multiphoton microscopy images, it was possible to calculate parameters like diameter, tortuosity and fiber orientation of the two structure proteins. Additionally, these parameters got statistically analysed.

4.1. Confocal microscopy

The literature review which is summarized in Table 2.3 does not allow a general statement on an ideal excitation and emission wavelength. However, all but one (O'Connel et al., 2008) of the authors agree that the excitation wavelength for collagen is lower than for elastin. Interestingly, the recommended ranges for the excitation of both proteins showed a strong variance. These proposals did not bring satisfying results at all.

Therefore, a porcine sample was taken and the autofluorescence wavelength of each possible excitation wavelength was measured. The result depicted in Figure 3.1(b) was the one, in which the structure of the tissue was visible best. The settings with which this image was obtained, were combined excitation wavelengths of 458, 476 and 561 nm. The author is of the opinion that both collagen and elastin were stimulated and thus this good autofluorescence was achieved.

To achieve a clear differentiation in this experimental environment, the test was repeated with human tissue. The test was performed for the pure collagen as well as for the pure elastin sample with all wavelengths. Thus, for collagen an excitation wavelength of 514 nm and for elastin 561 nm (Figure 3.2) the most intense autofluorescence image was obtained. The emission spectrum of collagen and elastin was measured utilizing a lambda-scan. Collagen has its emission peak at 567 nm and elastin showed the maximum at 590 nm.

Finally, the intensity of collagen and elastin autofluorescence was compared. Therefore, the autofluorescence intensity was calculated (Equation 2.1) with a background correction. A *photon count*-measurement was performed at the same wavelength and laser power for

both, collagen and elastin sample. In the elastin tissue in Figure 3.4, it is even optically visible that the amount of excited photons is higher than the one in collagen in Figure 3.5. The diagram in Figure 3.6 indactes a higher autofluorescence intensity at elastin tissue. These results are consistent with those of Fitzmaurice et al. (1989) and Richards-Kortum and Sevick-Muraca (1996) and were confirmed with another calculation method (Figure 3.7).

With the help of confocal microscopy and microspheres, the global and local stretch conditions got analysed. This analysis was carried out to obtain information about the strain conditions in the tissue. If the elongation was increased by the biaxial extension machine, firstly the linear positioner performs this change. By this change of position, a stretch is exerted on the tissue which is transmitted via the load cells, hooks and the suture thread to the tissue. The global stretch is defined by the biaxial extension machine. The global stretch describes the stretch applied to the tissue on the outer sides. To see if the tissue is evenly distributed under this extension, the local stretch is measured in the middle of the sample. It was therefore necessary to check whether a stretch change applied by the linear positioner (global stretch) also results in the same change in the middle of the tissue (local stretch).

To analyse the results in axial direction of the porcine aorta (Figure 3.9) the linear regression of all data points is considered. The value of local stretch is slightly below the value of global stretch. The ratio of global and local stretch in circumferential direction is nearly identical. This finding indicates that the tissue has a higher elasticity in the circumferential direction than in the axial direction. This is also consistent with the fact that in the physiological state a greater deformation occurs in the circumferential direction. As a result, the tissue must also be more elastic in this direction. The only limitation is that it was only possible to measure up to a stretch of 12%, because the microspheres then moved away from the visible area. A further statement can also be made about the condition of the deformation in the middle of the tissue. The change in global and local stretch values are nearly identical in both directions. This shows a very smooth stretching of the machine from all four sides.

During using the microspheres it was noticeable that *TetraSpeck Fluorescent Microsphere Standards* is not suitable for all kind of tissues. Throughout the experiments with porcine samples, the microspheres were always easy to detect. When switched to human media tissue only, no signal could be detected from them. In human adventitia tissues, however, the beads were detectable again. This could mean that a human media has a too solid histological structure to allow the microspheres to penetrate the tissue.

4.2. Confocal Reflection Microscopy

In order to investigate the possibility of a reflection microscopy signal, a porcine adventitia and media got examined. In Figure 3.11 and Figure 3.12 the difference between the reflective microscopy signal and the autofluorescence signal is obvious. The analysis of the elastase- and collagenase-treated samples in Figure 3.14 and Figure 3.16 confirms Jawerth et al. (2010) opinion that only collagen fibers can be detected by refelction microscopy.

The sample treated with elastase (Figure 3.14) showed two very strong signals in reflection and autofluorescence mode. As mentioned by Jawerth et al. (2010) and Artym and Matsumoto (2010) only fibers under $50°$ from the image plan give a strong signal. The reflection image in Figure 3.14(a) shows different brightness steps within the image whereas the autofluorescence image has a uniform brightness of the signal. This observation proves the dependence on orientation again.

The collagenase treated sample, on the contrary shows barely any signal. Just a few photons get detected here, but they could have their origins in artifacts. These results lead to the conclusion that reflective microscopy can be used to differentiate between elastin and collagen structures. If one takes a look at the porcine media sample microscopy image (Figure 3.14) again, it can be assumed that the areas only visible in the autofluorescence image are elastin structures. The collagen structures in both, media and adventitia sample, show their typical arrangement, which was also shown by Zeinali-Davarani et al. (2015), for example. Something essential should be mentioned at this point. In contrast to the usual structure of an untreated healthy medium, an elastase or collagenase treatment also changes the structure of the remaining collagen or elastin (Chow et al., 2014; Schriefl et al., 2016). To show this behavior, images Figure 3.13 and Figure 3.15 were taken with a brightfield microscope and picrosirius red-staining of the tissue. As one can see, the tissue is no longer in its original structure, but it is pure what makes the analysis for differentiation possible in the first place.

4.3. Multiphoton microscopy

In this last section of the master thesis, all data calculated from the images taken during the biaxial tensile test with a multiphoton microscope are discussed. These data are the Cauchy stress - stretch diagrams, diameter, tortuosity, and amplitude as well as the parameters of fiber orientation.

Figure 3.18, Figure 3.19 and Figure 3.20 show the aortic biaxial properties of human atherosclerotic and aneurysmatic tissue. All tested aortas show a typical exponential increase of stiffness with increasing stretch in the Cauchy stress-stretch diagrams. This applies both to the axial and circumferential direction of all aortas. This exponential course indicates the anisotropy and non-linearity of the tissue. If one looks at the curves in circumferential and axial direction separately, one notices that all three samples are stiffer in axial direction. This behavior can be described as physiological because during systole the aorta stretches more in circumference than in axial direction. As a result, the tissue must be more elastic in the circumferential direction. This behavior can also be seen in the Cauchy stress-stretch diagrams. The amount and orientation of collagen and elastin in the tissue determine the mechanical structure of arteries (Kamenskiy et al., 2014). At low stretch levels, elastin bears the load because the collagen fibers are still wrinkled. At higher stretch levels the collagen becomes straight and the stiffness increases.

The non-characteristic steps in Cauchy stress-stretch course are also conspicuous. How-

ever, these are because the tissue is relieved after a certain time after the stretch has been increased. This phenomena is called tissue relaxation and was already shown by Cavinato et al. (2017) with porcine arteries. In the case of this thesis, the sample was therefore left at a stretch level for so long to complete multiphoton imaging. Compared to healthy abdominal aortic media tests, shown by Schriefl et al. (2016), the response in axial and circumferential response of the pathological samples is stiffer than the healthy ones. The results are consistent with those of Holzapfel et al. (2004). The two atherosclerotic media samples (Figure 3.18, Figure 3.19) were obtained from the same person, but because they were located elsewhere in the aorta, they have different characteristics. If the two are compared at a stretch value of 15%, the first sample got a stress of 11 kPa in circumferential direction and 9 kPa in axial direction. The second one is more elastic in both directions with stresses of 22 kPa and 18 kPa, respectively. This shows that the condition of arteriosclerosis is locally variable and does not affect the entire aorta in equal parts. The sample with an abdominal atherosclerotic aneurysm (Figure 3.20) is even stiffer compared to the atherosclerotic ones. The peak values at 30% stretch are much smaller in circumferential direction as well as in axial direction for the aneurysmatic tissue. These observations are similar to those of Niestrawska et al. (2016).

One of the limitations of the complicated experimental set-up with the machine above the multiphoton laser becomes apparent here. One of the tests had to be aborted at a stretch level of 18%. In an attempt to focus the laser correctly into the tissue, a cover glass is placed on it. In order not to falsify the mechanical properties, the cover glass is only held on the specimen by adhesion forces. By a change of the structure of the sample due to diseases, by drying out, or by the tensile forces of the biaxial extension machine, this cover glass can become detached. If one of these problems occurs, the cover glass usually falls on the lens and therefore no further image can be taken.

In this part of the discussion, the measured parameters of the samples are examined for similarities, differences, and irregularities. Initially, all samples will be analysed individually. The collected data describe two atherosclerotic elastin fibers, one aneurysmatic elastin, and one atherosclerotic collagen fiber. Unfortunately, it was not possible to record both channels (with appropriate wavelength detection) for elastin and collagen in the desired quality for each sample. Reasons for this could be changes in the tissue due to the storage process, pathological changes in the tissue, or background light that disturbs the detector. Besides, the sample dries out due to the high intensity of the multiphoton laser. As already mentioned, the autofluorescence wavelengths of collagen and elastin are close together, and as has been proven, elastin has a stronger autofluorescence. All these factors can lead to problems in the signal acquisition.

The first proteins to be analysed are the elastin fibers from atherosclerotic tissue. The diameter of the fibers (Figure 3.21) seems to be on a constant value in the beginning but then suddenly drop during the stretch increase from 16% to 18%. The Mann-Whitney U test also indicates a change at this spot (Table A.3). The amplitude of elastin is going down quite linear from $5\,\mu m$ to $1.5\,\mu m$, only the last three values show a noticeable difference

both in the diagram and in the statistical elaboration (Figure 3.23, Table A.3). In the case of tortuosity, there is no tendency to see what might have to do with the difficult measurement procedures. The Mann-Whitney U test indicates that the distribution of fiber angle ϕ and the dispersion coefficient κ_{ip} are similar with increasing strain. The second atherosclerotic elastin media sample shows a similar behavior in elastin diameter. It starts at around $5\mu m$ and stays quite constant (Figure 3.22). The Mann-Whitney U test (Table A.4) reveals no abnormalities, too. Although the test reveals that the tortuosity and amplitude do not have the same distribution, beginning with a stretch value of 10% and 13%, respectively. The intensity plot in Figure 3.29 presents a widely distribution of ϕ in the beginning, with increasing stretch the fibers tend to be better aligned. Mann-Whitney U test also shows that there is a change in ϕ and κ_{ip}, beginning at 14%. Since the data are widely distributed in the beginning, this indicates that the fibers become more aligned. The Spearman rank correlation in Table A.8 calculates a high covariance between diameter and tortuosity, amplitude and diameter as well as tortuosity and amplitude.

The diameter of elastin from the aneurysmatic media remains at an approximately constant value again before it is reduced sharply, but in contrast to the other elastin fibers it is smaller with starting at $2.75\,\mu m$. Considering the fluctuation range due to the resolution, this result nevertheless seems reasonable. The Mann-Whitney U test indicates a change after a stretch level of 22%, too. The tortuosity shows the same behavior as the atherosclerotic samples before. Intensity plot in Figure 3.30 demonstrates that from an initial strong dispersion of fiber direction, the fibers gradually move again in a certain direction and become better aligned. However, the Mann-Whitney U test indicates that almost all values for the dispersion coefficient κ_{ip} differ from the previous one. The Spearman rank sum test states that the diameter, tortuosity and amplitude show a high correlation among themselves again.

Finally, the characteristics for atherosclerotic collagen fibers are explained, starting with the diameter in Figure 3.21. It is noticeable that collagen fibers are thicker than those of elastin and that the course decreases almost linearly. Exceptions are both in the places of 6% and 16%, as the Mann-Whitney U test proves (Table A.2). Amplitude and tortuosity (Figure 3.24) decrease evenly at the beginning, but start to differ from the previous values at stretch levels of 20% and 10%, respectively. In absolute values, both amplitude and tortuosity show the maximum values of all data. The dispersion coefficient κip stays quite constant, the fiber angle ϕ is again widely distributed at the initial state and aligns with increasing stretch levels into one direction. The Mann-Whitney U test also says that these two parameters change equally. Once again tortuosity, amplitude and diameter are strong monotonically related.

Summary   In summary, it can be said that it is not possible with confocal microscopy to visualize collagen or elastin fibers just by changing the excitation wavelength. The excitation and emission spectra of the two proteins are too closely related. It is not possible with the confocal microscopy method by just changing the excitation and emission wavelengths to distinguish between them. On the contrary, it was proven that that elastin shows a higher autofluorescence intensity than collagen. Confocal microscopy images of tissue

stained with microspheres demonstrated that at least up to a value of 12 percent the biaxial machine ensures homogeneous distribution of the stretch level.

Confocal reflection microscopy can be used to gather additional information about collagen tissue with relatively little extra effort during using confocal microscopy methods. Elastin tissue does not generate a reflection microscopy image at all. This allows additional collagen tissue to be discovered. However, it has the disadvantage that only fibers with a certain orientation are visible. If there is an additional possibility to examine the tissue with a multiphoton microscope, this method can be considered redundant.

The evaluation of multiphoton microscopy images enabled information about the structure parameters diameter, amplitude, tortuosity, fiber angle, and dispersion coefficient. The expected behavior of Cauchy stress-stretch diagrams exposes no abnormalities. The mechanical behavior of atherosclerotic tissue is shown to be more elastic than that of aneurysmatic tissue. With the Spearman rank sum correlation, it was shown that there is a strong monotonic relation between amplitude, diameter and waviness. This remarkable feature was found in all tested samples; this applies to both elastin and collagen fibers. The changes in height and the course of diameter, tortuosity and amplitude with increasing stretch are very similar for all measured elastin samples. The values for collagen are higher for all measured parameters. The Mann-Whitney U test can be said to be extremely helpful in highlighting spontaneous differences in one of the parameters. Often the assumptions that stood out from the measured parameters were confirmed by the test. However, as these are only a small number of samples, these statistical statements should be taken with caution.

Bibliography

G. A. Holzapfel, G. Sommer, and P. Regitnig. Anisotropic mechanical properties of tissue components in human atherosclerotic plaques. *J. Biomech. Eng.*, 126:657–665, 2004.

G. Knner, B. E. RolfeJ. H. Campbell, S. J. Parkin, N. R. Heckenburg and H. Rubinsztein-Dunlop. Mechanics of Cellular Adhesion to Artificial Artery Templates. *Biophys. J.*, 91: 3085–3096, 2006.

A. I. Arroyave, R. G. Lima, P. A.LS. Martins, N. Ramiao, and R. M. N. Jorge. Methodology for Mechanical Characterization of Soft Biological Tissues: arteries *Procedia. Eng.*, 110:74–81, 2015.

G. A. Holzapfel, T. C. Gasser, and R. W. Ogden A New Constitutive Framework for Arterial Wall Mechanics and a Comparative Study of Material Models. *J. Elast.*, 61: 1–48, 2000.

G. Wang, M. Garcia, X. Lu, Y. Lanir and G. S. Kassab Three-dimensional mechanical properties of porcine coronary arteries: a validated two-layer model *Am. J. Physiol. Heart Circ. Physiol.*, 291:H1200–H1209, 2006.

R. R. Alfano and Y. Yang. Stokes Shift Emission Spectroscopy of Human Tissue and Key Biomolecules. *IEEE J. Sel. Top. Quantum Electron*, 9(2):148–153, 2003.

User Manual - Leica TCS SP5. Leica Microsystems CMS GmbH (GER). $http://www3.unifr.ch$ *[cited 20 Apr. 2019]* Available from: https: $//www3.unifr.ch/bioimage/wp - content/uploads/2013/10/User - Manual\_TCS\_SP5\_V02\_EN.pdf$

User Manual - TetraSpeckTM Fluorescent Microsphere Standards. Molecular Probes, Inc. (UK). $http://www.thermofischer.com$ *[cited 6 Jun. 2019]* Available from: https: $//www.thermofisher.com/document - connect/document - connect.html?url = https\%3A\%2F\%2Fassets.thermofisher.com\%2FTFS - Assets\%2FLSG\%2Fmanuals\%2Fmp07279.pdf$

G. A. Holzapfel, T. C. Gasser, and R. Stadler A structural model for the viscoelastic behavior of arterial walls: Continuum formulation and finite element analysis. *Eur. J. Mech. A Solids*, 21(3):441–463, 2001.

User Manual - Leica TCS SP5. Leica Microsystems CMS GmbH (GER). *http://i-med.ac.at [cited 20 Apr. 2019]* Available from: https: $//www.i-med.ac.at/neurobiochemistry/neurobiochemistry/Biooptics/Documents\_pdf/Leica-HyD-Brochure\_EN.pdf$

L. M. Jawerth, S. Mnster, D. A. Vader, B. Fabry and D. A. Weitz A Blind Spot in Confocal Reflection Microscopy: The Dependence of Fiber Brightness on Fiber Orientation in Imaging Biopolymer Networks. *Biophys. J.*, 98:L01-L03, 2010.

V. V. Artym and K. Matsumoto. Imaging Cells in Three-Dimensional Collagen Matrix. *Current Protocols in Cell Biology*, 48(1):10.18.1–10.18.20, 2010.

A. O. Brightman, B. P. Rajwa, J. E. Sturgis, M. E. McCallister, J. P. Robinson and S. L. Voytik-Harbin. Timelapse confocal reflection microscopy of collagen fibrillogenesis and extracellular matrix assembly in vitro. *Biopolymers*, 54(3):222-234, 2000.

M. Fitzmaurice, J.O. Bordagaray, G. L. Engelmann, R. Richards-Kortum, T. Kolubayev, M. S. Feld, N. B. Ratliff and J. R. Kramer. Argon ion laser-excited autofluorescence in normal and atherosclerotic aorta and coronary arteries: Morphologic studies. *Am. H .J*, 118(5):1028–1088, 1989.

R. Richards-Kortum and E.Sevick-Muraca Quantitative optical Spectroscopy for Tissue Diagnosis. *Annu. Rev. Phys. Chem.*, 47:555–606, 1996.

A. Burges, R. A, McCloy, S. Rogers, C. E. Caldon, T. Lorca and A. Castro Partial inhibition of Cdk1 in G2 phase overrides the SAC and decouples mitotic events. *Cell Cycle*, 13(9): 1400–1412, 2014.

Z.Deyl, K. Macek, M. Adam and Vancikova. Studies on the chemical nature of elastin fluorescence. *Biochimica et Biophysica Acta*, 625:248–254, 1980.

E. M. Gill, A. Malpica, R. E. Alford, A. R. Nath, M. Follen, R. Richards-Kortum and N. Ramanujam Relationship Between Collagen Autofluorescence of the Human Cervix and Menopausal Status. *Photochemistry and Photobiology*, 77(6):653–658, 2003.

M. K. O'Connel, S. Murthy, S. Phan, C. Xu, J. Buchanan, R. Spilker, R. L. Dalman, C. K. Zarins, W. Denk and C. A. Talyor The three-dimensional micro- and nanostructure of the aortic medial lamellar unit measured using 3D confocal and electron microscopy imaging. *Matrix Biol.*, 27:171–181, 2008.

A. C. Croce and G. Bottrill. Autofluorescence spectroscopy and imaging: a tool for biomedical research and diagnosis. *Eu. J. Histochem.*, 58:320–337, 2014.

E. A. Stephen, A. Venkatasubramaniam, T. A. Good and L. D. Topoleski. The effect of glycation on arterial microstructure and mechanical response. *Society for Biomaterials* [published online] https: $//onlinelibrary.wiley.com/doi/pdf/10.1002/jbm.a.34927$

H. L. Zhao, C. P. Zhang, H. Zhu, Y. F. Jiang and X. B. Fu Autofluorescence of collagen fibers in scar. *Skin, Research and Technology*, 23(4):588–592, 2017.

S. Zeinali-Davarani, Y. Wang, M. J. Chow, R.Turcotte and Y.Zhang Contribution of Collagen Fiber Undulation to Regional Biomechanical Properties Along Porcine Thoracic Aorta. *J. Biomech. Eng.*, 137(5):051001-1–051001-10, 2015.

M. J. Chow, R. Turcotte, C. P. Lin and Y. Zhang Arterial Extracellular Matrix: A Mechanobiological Study of the Contributions and Interactions of Elastin and Collagen. *Biophys. J.*, 106:26842692, 2014

A. J. Schriefl , T. Schmidt, D. Balzani, G. Sommer a, G. A. Holzapfel Selective enzymatic removal of elastin and collagen from human abdominal aortas: Uniaxial mechanical response and constitutive modeling. *Acta Biomater.*, 17:125-136, 2015

J. D. Humphrey, R. K. Strumpf, and F. C.P. Yin Biaxial mechanical behavior of excised ventricular epicardium. *Am. J. Physiol.* 259:H101-H108, 1990

C. Towler. Quantification of Fibre Waviness in Healthy and Diseased Abdominal Aortas. Master's thesis, University of Glasgow, Glasgow, School of Engineering, Graz, 2017.

S. Sherifova, G. Sommer, C. Viertler, P. Regitnig, T. Caranasos, M. A. Smith, B. E. Griffith, R. W. Ogden, G. A. Holzapfel. Failure Properties and Microstructure of Healthy and Aneurysmatic Human Thoracic Aortas Subjected to Uniaxial Extension with a Focus on the Media. *Acta Biomater.* : Preprint, 2019

J. A. Niestrawska1, C. Viertler, P. Regitnig, T .U. Cohnert, G. Sommer and G. A. Holzapfel. Microstructure and mechanics of healthy and aneurysmatic abdominal aortas: experimental analysis and modelling *J. R. Soc. Interface* 13:20160620, 2016.

F. Zehentner Transfer of Sourcecode to JAVA for Implementation of Angular Dispersion Analysis Plug-in into ImageJ Master's thesis, University of Technology, Graz, and Institute of Biomechanics Graz, 2018

A. J.Schriefl, A. J.Reinisch, S. Sankaran, D. M. Pierce and G. A. Holzapfel. Quantitative assessment of collagen fiber orientations from two-dimensional images of soft biological tissues *J. R. Soc. Interface* 9:3081-3091, 2012.

Wayne W. LaMorte. Boston University School of Public Health [Internet] *http://sphweb.bumc.bu.edu [cited 1 Sept. 2019]* Available from: $http://sphweb.bumc.bu.edu/otlt/mph - modules/bs/bs704\_nonparametric/BS704\_Nonparametric4.html$

John H. McDonald. Handbook of Biological Statistics (3rd ed.) pages 209–212, *Sparky House Publishing* Baltimore, Maryland, 2014.

A. V. Kamenskiy, Y. A. Dzenis, S. A. Jaffar Kazmi, M. A. Pemberton, I. I. Pipinos, and
   N. Y. Phillips. Biaxial mechanical properties of the human thoracic and abdominal aorta,
   common carotid, subclavian, renal and common iliac arteries. *Biomech. Model. Mechan.*
   13:1341-1359, 2014.

G. A. Holzapfelel, G. Sommer, and P. Regitnig. Anisotropic Mechanical Properties of
   Tissue Components in Human Atherosclerotic Plaques. *J. Biomech. Eng.* 26(5):657,
   2004.

C. Cavinato, C. Helfenstein-Didier, T. Olivier, S. Rolland du Roscoat, N. Laroche and
   P. Badel Biaxial loading of arterial tissues with 3D in situ observations of adventitia
   fibrous microstructure: A method coupling multi-photon confocal microscopy and bulge
   inflation test. *J. Mech. Behav. Biomed. Mater.* 74:488–498, 2017.

W. Denk and W. W. Strickler. Two-photon laser scanning fluorescence microscopy. *Science*, 248:73–76, 1990.

Appendices

A. Tables

A.1. Data from local and global stretch analysis

Table A.1 shows the data recorded of microsphere position during the tensile test. The different microspheres are called *B0* to *B9*. The columns show the change of x-and y-position due to the elongation of the sample and depending on the picture. Every row indicates the new position on the following image after an 0.02 increment of the global stretch.

Table A.1   Position of different microsphere beads at different steps of extension

Stretch	B0		B1		B2		B3		B4		B5		B6		B7		B8		B9	
	X	Y	X	Y	X	Y	X	Y	X	Y	X	Y	X	Y	X	Y	X	Y	X	Y
0%	68	251	228	159	255	167	222	204	180	304	65	378	173	432	305	293	45	495	234	408
2%	100	221	263	129	290	139	256	178	213	280	96	354	208	411	341	268	74	475	268	386
4%	118	203	283	107	311	120	274	158	234	260	113	337	225	394	361	250	88	460	288	367
6%	146	182	313	83	342	95	307	132	262	239	139	316	253	374	392	226	115	442	317	345
8%	163	170	332	73	363	82	323	121	282	226	156	304	271	363	411	214	130	435	335	335
10%	180	161	348	62	383	72	343	110	299	215	172	300	287	359	430	205	144	427	351	327
12%	149	161	318	66	351	70	311	109	268	221	140	305	256	365	403	210	112	436	323	337

A.2. Data from Mann-Whitney U test

The following tables conatin the results of the Mann-Whitney U test. A '1' indicates $H = 1$ and stands for a rejection of the null hypothesis. '0' stands for $H = 0$ and means the null hypothesis is approved.

Table A.2   Analysis of measured and calculated collagen data from the human atheroscle-
rotic tissue. (Person #3, Sample 1)

Stretch comp.	Diameter	Amplitude	Tortuosity	κ_{ip}	ϕ
0 vs 2%	0	0	0	0	0
2% vs 4%	0	0	0	0	0
4% vs 6%	0	0	0	0	0
6% vs 8%	1	0	0	0	0
8% vs 10%	0	0	0	0	0
10% vs 12%	0	0	1	0	0
12% vs 14%	0	0	0	0	0
14 % vs 16%	0	0	1	0	0
16% vs 18%	1	0	1	0	0
18% vs 20%	0	0	0	0	0
20% vs 22%	0	1	1	0	0
22% vs 24%	0	1	1	0	0
24% vs 26%	0	1	1	0	0
26% vs 28%	0	1	1	0	0
28% vs 30%	0	1	1	0	0

Table A.3   Analysis of measured and calculated elastin data from the human atheroscle-
rotic tissue. (Person #3, Sample 1)

Stretch comp.	Diameter	Amplitude	Tortuosity	κ_{ip}	ϕ
0 vs 2%	0	0	0	0	0
2% vs 4%	0	0	0	0	0
4% vs 6%	0	0	0	0	0
6% vs 8%	0	0	0	0	0
8% vs 10%	0	0	1	0	0
10% vs 12%	0	0	0	0	0
12% vs 14%	0	0	1	0	0
14 % vs 16%	0	0	1	1	0
16% vs 18%	1	0	1	0	0
18% vs 20%	0	0	1	0	0
20% vs 22%	0	0	1	0	0
22% vs 24%	0	0	1	0	0
24% vs 26%	0	1	1	0	0
26% vs 28%	0	1	1	0	0
28% vs 30%	0	1	1	0	0

Table A.4   Analysis of measured and calculated elastin data from the human atheroscle-
rotic tissue. (Person #3, Sample 2)

Stretch comp.	Diameter	Amplitude	Tortuosity	κ_{ip}	ϕ
0 vs 2%	0	0	0	0	0
2% vs 4%	0	0	0	0	0
4% vs 6%	0	0	0	0	0
6% vs 8%	0	0	0	0	0
8% vs 10%	0	0	1	0	0
10% vs 12%	0	1	1	0	0
12% vs 14%	0	1	1	0	0
14 % vs 16%	0	1	1	1	1
16% vs 18%	0	1	1	1	1

Table A.5   Analysis of measured and calculated elastin data from the human aneurysmatic tissue. (Person #2)

Stretch comp.	Diameter	Amplitude	Tortuosity	κ_{ip}	ϕ
0 vs 2%	0	0	0	0	0
2% vs 4%	0	0	0	1	0
4% vs 6%	0	0	0	0	0
6% vs 8%	0	0	0	1	1
8% vs 10%	0	1	0	1	0
10% vs 12%	0	1	1	1	0
12% vs 14%	0	1	1	1	0
14 % vs 16%	0	1	1	1	0
16% vs 18%	0	1	1	1	0
18% vs 20%	0	1	1	1	0
20% vs 22%	0	1	1	1	0
22% vs 24%	1	1	1	0	0
24% vs 26%	0	1	1	1	0
26% vs 28%	0	1	1	1	0
28% vs 30%	0	1	1	1	0

A.3. Data from Spearman rank correlation

The tables listed below show the results of the Spearman rank correlation test. The table features the $\rho-$value and its corresponding $p-$value for every analysed tissue. A '*' next to the $\rho-$value indicates that there is no correlation because $p > 0.05$.

Table A.6   Spearman rank correlation coefficients for atherosclerotic collagen sample. (Person #3, Sample 1)

	Diameter		Tortuosity		Amplitude		κ_{ip}	
	ρ	p	ρ	p	ρ	p	ρ	p
Tortuosity	0.963	0.015	-	-	-	-	-	-
Amplitude	0.952	0.014	0.970	0.032	-	-	-	-
κ_{ip}	0.027*	0.925	-0.059*	0.830	0.016*	0.95	-	-
ϕ	0.827	0.047	0.832	0.024	0.837*	0.964	0.015	0.014

Table A.7   Spearman rank correlation coefficients for atherosclerotic elastin sample. (Person #3, Sample 1)

	Diameter		Tortuosity		Amplitude		κ_{ip}	
	ρ	p	ρ	p	ρ	p	ρ	p
Tortuosity	0.703	0.015	-	-	-	-	-	-
Amplitude	0.735	0.017	0.944	0.042	-	-	-	-
κ_{ip}	0.356*	0.176	0.744	0.001	0.782	0.012	-	-
ϕ	0.388*	0.138	0.352 *	0.184	0.409*	0.096	0.432	0.014

Table A.8   Spearman rank correlation coefficients for atherosclerotic elastin sample. (Person #3, Sample 2)

	Diameter		Tortuosity		Amplitude		κ_{ip}	
	ρ	p	ρ	p	ρ	p	ρ	p
Tortuosity	0.927	0.013	-	-	-	-	-	-
Amplitude	0.985	0.023	0.960	0.010	-	-	-	-
κ_{ip}	0.370*	0.296	0.188*	0.607	0.334*	0.345	-	-
ϕ	0.406*	0.246	0.588	0.0403	0.505*	0.137	-0.261*	0.470

Table A.9   Spearman rank correlation coefficients for aneurysmatic elastin sample. (Person #2)

	Diameter		Tortuosity		Amplitude		κ_{ip}	
	ρ	p	ρ	p	ρ	p	ρ	p
Tortuosity	0.962	0.010	-	-	-	-	-	-
Amplitude	0.921	0.005	0.935	0.012	-	-	-	-
κ_{ip}	0.106*	0,697	-0.129*	0,632	0.012*	0,169	-	-
ϕ	0.538	0,033	0.615 *	0,0131	0.571	0,023	0.400*	0,125

A.4. Data from fiber orientation

The tables show the median values for the median fiber angle ϕ and the dispersion coefficient κ_{ip}. Additionally the lower and upper quartile is listed. The sample number for the calculation of ϕ and κ_{ip} was 5 for every sample.

Table A.10   Median value, lower (Q1) and upper (Q3) quartile of structural parameters (ϕ, κ_{ip}) of atherosclerotic collagen fibers. (Person #3, Sample 1)

Stretch	Median(ϕ)[°]	[Q1;Q3]	Median(κ_{ip})[-]	[Q1;Q3]
1.00	-0.7	[-1.3; 0.3]	0.453	[0.187; 0.467]
1.02	0.8	[-1.1; 1.6]	0.463	[0.454; 0.468]
1.04	-0.3	[-1.3; 1.3]	0.456	[0.451; 0.463]
1.06	-0.9	[-1.3; 0.3]	0.456	[0.454; 0.459]
1.08	-1.2	[-3.5; -1.1]	0.454	[0.454; 0.461]
1.10	-0.7	[-1.6; 0.4]	0.449	[0.448; 0.456]
1.12	0.0	[-2.1; 2.5]	0.456	[0.444 ; 0.459]
1.14	-1.6	[-1.8; -1.5]	0.447	[0.439; 0.450]
1.16	0.1	[-0.2; 0.3]	0.432	[0.429; 0.436]
1.18	-0.2	[-0.9; 0.8]	0.433	[0.432; 0.434]
1.20	-0.5	[-1.8; -0.3]	0.418	[0.416; 0.424]
1.22	-0.8	[-4.1; -0.6]	0.423	[0.421; 0.428]
1.24	-3.5	[-4.8; -0.3]	0.421	[0.417; 0.433]
1.26	-1.0	[-3.3; -0.7]	0.421	[0.416; 0.427]
1.28	-0.6	[-5.8; -0.5]	0.421	[0.418; 0.432]
1.30	-3.0	[-4.6; -0.3]	0.424	[0.150; 0.434]

Table A.11   Median value, lower (Q1) and upper (Q3) quartile of structural parameters (ϕ, κ_{ip}) of atherosclerotic elastin fibers. (Person #3, Sample 1)

Stretch	Median(ϕ)[°]	[Q1;Q3]	Median(κ_{ip})[-]	[Q1;Q3]
1.00	7.8	[-1.1;7.9]	0.291	[0.278; 0.393]
1.02	5.0	[3.3;7.7]	0.389	[0.297; 0.405]
1.04	3.7	[2.6;5.5]	0.400	[0.273; 0.406]
1.06	2.5	[2.5; 8.8]	0.402	[0.399; 0.405]
1.08	2.6	[1.3; 5.0]	0.383	[0.131; 0.398]
1.10	1.5	[1.4; 3.6]	0.142	[0.126;0.389]
1.12	0.1	[-3.7; 1.9]	0.279	[0.267; 0.386]
1.14	0.7	[0.6; 1.9]	0.178	[0.123; 0.385]
1.16	0.9	[0.6; 1.7]	0.132	[0.132; 0.140]
1.18	0.2	[0.0; 0.4]	0.376	[0.148; 0.377]
1.20	-0.5	[-1.1; 0.8]	0.369	[0.143; 0.377]
1.22	-0.5	[-0.8; -0.4]	0.146	[0.139; 0.366]
1.24	-0.7	[-0.9; -0.5]	0.122	[0.121; 0.125]
1.26	-1.6	[-1.7; 0.2]	0.177	[0.127; 0.368]
1.28	-1.0	[-1.5; -0.1]	0.132	[0.127; 0.377]
1.30	-1.4	[-2.1; -0.3]	0.134	[0.130; 0.372]

Table A.12   Median value, lower (Q1) and upper (Q3) quartile of structural parameters (ϕ, κ_{ip}) of atherosclerotic elastin fibers. (Person #3, Sample 2)

Stretch	Median(ϕ)[°]	[Q1;Q3]	Median(κ_{ip})[-]	[Q1;Q3]
1.00	-13.1	[-21.1;-11.9]	0.460	[0.454 ; 0.469]
1.02	23.6	[-16.0;24.1]	0.376	[0.373; 0.457]
1.04	-3.2	[-5.6;17.5]	0.453	[0.442; 0.463]
1.06	-15.1	[-26.8;-7.2]	0.437	[0.424; 0.455]
1.08	21.2	[-9.3;27.3]	0.439	[0.423; 0.451]
1.10	-5.3	[-25.4;15.2]	0.446	[0.337; 0.449]
1.12	12.0	[-11.7;14.0]	0.453	[0.417; 0.457]
1.14	-28.3	[-48.0;-25.5]	0.423	[0.407; 0.437]
1.16	-32.1	[-33.0 ;-10.2]	0.454	[0.447; 0.464]
1.18	-34.9	[-52.4;-23.1]	0.427	[0.412; 0.444]

Table A.13   Median value, lower (Q1) and upper (Q3) quartile of structural parameters
             (ϕ, κ_{ip}) of aneurysmatic elastin fibers. (Person #2)

Stretch	Median(ϕ)[°]	[Q1;Q3]	Median(κ_{ip})[-]	[Q1;Q3]
1.00	39.1	[27.5; 39.2]	0.413	[0.413; 0.464]
1.02	22.7	[22.6; 25.8]	0.456	[0.452; 0.462]
1.04	25.6	[21.8; 26.7]	0.462	[0.442; 0.474]
1.06	30.6	[12.7; 33.2]	0.387	[0.381; 0.456]
1.08	18.1	[12.5; 20.7]	0.469	[0.464; 0.481]
1.10	-1.3	[-7.8; 10.2]	0.456	[0.453; 0.462]
1.12	-8.6	[-9.0; -8.1]	0.467	[0.456; 0.468]
1.14	-11.2	[-11.8; -10.4]	0.460	[0.459; 0.473]
1.16	-7.8	[-8.8; 1.2]	0.471	[0.458; 0.480]
1.18	-9.1	[-9.4; -6.9]	0.458	[0.456; 0.458]
1.20	-8.8	[-9.0; -8.3]	0.461	[0.457; 0.462]
1.22	-10.0	[-10.8; -9.3]	0.465	[0.450; 0.467]
1.24	-9.0	[-9.3; 15.9]	0.451	[0.441; 0.472]
1.26	-11.4	[-12.3; -11.3]	0.468	[0.439; 0.468]
1.28	-14.7	[-16.4; -9.5]	0.459	[0.434; 0.472]
1.30	-16.7	[-17.6; -10.0]	0.454	[0.438; 0.472]